

1 Multi-fold increase in rainforests tipping risk beyond 1.5-2°C warming

2 Chandrakant Singh^{1,2,3,*}, Ruud van der Ent⁴, Ingo Fetzer^{1,2,5}, Lan Wang-Erlandsson^{1,2,5}

3 ¹Stockholm Resilience Centre, Stockholm University, Stockholm, Sweden

4 ²Bolin Centre for Climate Research, Stockholm University, Stockholm, Sweden

5 ³Department of Space, Earth and Environment, Chalmers University of Technology, Gothenburg, Sweden

6 ⁴Department of Water Management, Faculty of Civil Engineering and Geosciences, Delft University of Technology, Delft,
7 The Netherlands

8 ⁵Potsdam Institute for Climate Impact Research, Potsdam, Germany

9

10 *Corresponding author; E-mail: chandrakant.singh@su.se, chandrakant.singh@chalmers.se

11

12 ORCID

13 Chandrakant Singh: <http://orcid.org/0000-0001-9092-1855>

14 Ruud van der Ent: <https://orcid.org/0000-0001-5450-4333>

15 Ingo Fetzer: <http://orcid.org/0000-0001-7335-5679>

16 Lan Wang-Erlandsson: <http://orcid.org/0000-0002-7739-5069>

17

18 **Abstract.** Tropical rainforests rely on their root systems to access moisture stored in soil during wet periods for
19 use during dry periods. When this root-zone soil moisture is inadequate to sustain a forest ecosystem, they
20 transition to a savanna-like state, losing their native structure and functions. Yet the influence of climate change
21 on ecosystem's root-zone soil moisture storage and their impact on rainforest ecosystems remain uncertain. This
22 study assesses the future state of rainforests and the risk of forest-to-savanna transitions in South America and
23 Africa under four shared socioeconomic pathways (SSP1-2.6, SSP2-4.5, SSP3-7.0, and SSP5-8.5). Using a mass-
24 balance-based empirical understanding of root zone storage capacity (S_r), defined as the maximum volume of
25 root zone soil moisture per unit area accessible to vegetation's roots for transpiration, we project how rainforest
26 ecosystems will respond to future climate changes. We find that under the end-of-the-21st-century climate, nearly
27 one-third of the total forest area will be influenced by climate change. As the climate warms, forests will require
28 a larger S_r than they do under the current climate to sustain their ecosystem structure and functions, making them
29 more susceptible to water limitations. Furthermore, warming beyond 1.5-2°C will significantly elevate the risk
30 of a forest-savanna transition. In the Amazon, the forest area at risk of such a transition grows by about 1.7-5.8
31 times in size compared to the immediate lower warming scenario (e.g., SSP2-4.5 compared to SSP1-2.6). In
32 contrast, the risk growth in the Congo is less substantial, ranging from 0.7-1.7 times. These insights underscore
33 the urgent need to limit the rise of global surface temperature below the Paris Agreement to conserve rainforest
34 ecosystems and associated ecosystem services.

35 **1 Introduction**

36 Tropical rainforests in the Amazon and Congo basins are critical to the Earth system since they store and
37 sequester a large amount of carbon, host vast biodiversity, and regulate the global water cycle (Malhi et al., 2014).
38 However, these forests are under severe pressure from climate and land-use changes (Davidson et al., 2012;
39 Lewis et al., 2015; Malhi et al., 2008). These changes result in decreased precipitation, increased seasonality, and
40 higher atmospheric water demand (Malhi et al., 2014), leading to soil moisture deficits that inhibit plant growth
41 (Singh et al., 2020; Wang-Erlandsson et al., 2022). Furthermore, projected increases in drought frequency,
42 severity, and duration under future climate change (Dai, 2011; Liu et al., 2018) pose imminent threats to the
43 capacity of rainforests to maintain their native ecological structure and functions (i.e., forest resilience) (Bauman
44 et al., 2022; Grimm et al., 2013; Jones et al., 2009).

45 Under water-deficit conditions, rainforests adapt by investing in their root systems to gain better access to
46 soil moisture necessary to maintain their structure and functions (Singh et al., 2020, 2022). At the same time, the
47 availability of surplus moisture at shallow depths minimises the need for ecosystems to invest in extensive
48 (deeper and lateral) root systems (Bruno et al., 2006). Furthermore, forest ecosystems adapt to climate change by
49 optimising water distribution through mechanisms such as hydraulic redistribution (Liu et al., 2020; Oliveira et
50 al., 2005), enhancing water-use efficiency by regulating stomatal conductance, and even shedding leaves (Wolfe
51 et al., 2016) to minimise moisture loss (Barros et al., 2019; Brum et al., 2019; Lammertsma et al., 2011). Despite
52 their critical role, the dynamic influence of climate change on vegetation's rooting structure and subsoil moisture
53 is challenging to measure at the ecosystem scale (Fan et al., 2017). Thus, understanding how moisture from wet
54 periods is stored, transmitted, and lost from the soil, as well as how it is accessed by vegetation during dry periods,
55 is critical to the ecohydrology and resilience of terrestrial ecosystems under climate change.

56 However, such ecohydrological dynamics remain challenging to incorporate in Earth System Models
57 (ESMs) (Lenton, 2011; Maslin and Austin, 2012; Valdes, 2011) – complex mathematical representations of Earth
58 system processes and interactions across different biospheres. This limits the capacity of ESMs to simulate
59 tipping points as an emergent property of the system (i.e., properties that emerge due to multiple interactions
60 between several system components, and are not the property of an individual component) (Hirota et al., 2021;
61 Reyer et al., 2015; Singh et al., 2023). This constraint is mainly due to our poor understanding of complex
62 mechanisms governing the ecosystem, which are not well represented in ESMs. This includes a limited
63 understanding of vegetation-climate feedbacks (Boulton et al., 2013, 2017; Chai et al., 2021), subsoil moisture
64 availability (Cheng et al., 2017), ecosystem adaptation dynamics (Yuan et al., 2022), the response time of forest
65 ecosystems to climate change perturbations, and assumptions about future (i.e., prescribed) land-use change
66 (Hurtt et al., 2020) in the ESMs. Furthermore, in the Earth system, some interactions still remain largely
67 unknown, thereby making the prediction of (abrupt) forest-to-savanna transition (referring to changes in the
68 dense-canopy structure of forests to one that mimics an open-canopy structure similar to savanna; hereafter
69 referred to as forest-savanna transition) challenging (Drijfhout et al., 2015; Hall et al., 2019; Koch et al., 2021).

70 To understand the extent of rainforest tipping risks, there is a need to assess and contrast the forest
71 resilience consequences of low-emission and current commitment trajectories with the more commonly used
72 high-emission scenario (Jehn et al., 2022). However, the risk of forest-savanna transitions under various possible
73 climate future scenarios is relatively under-investigated. As a result of the conflicting findings and scenario-
74 dependent uncertainties, the Intergovernmental Panel on Climate Change (IPCC) has only low confidence about
75 the possible tipping of the Amazon forest by the end of the 21st century (Canadell et al., 2021). However, with
76 mounting empirical evidence on how climate change influences rainforest ecosystems (Boulton et al., 2022;
77 Küçük et al., 2022; Singh et al., 2020, 2022), the research on rainforest resilience loss has accelerated
78 considerably in the recent decade (Ahlström et al., 2017; Huntingford et al., 2013). Yet, forest resilience is often
79 assessed based on changes in forest carbon stocks (Huntingford et al., 2013; Parry et al., 2022) or precipitation
80 (Hirota et al., 2011; Staal et al., 2020; Zemp et al., 2017); and rarely on the subsoil moisture availability of the
81 ecosystem (Singh et al., 2022).

82 This study aims to assess the state of rainforests and the risk of a forest-savanna transition under the end
83 of the 21st-century climate based on an empirical understanding of ecosystems' root zone storage dynamics. For
84 this, we use mass-balance derived root zone storage capacity (S_r) – representing the maximum amount of soil
85 moisture vegetation can access for transpiration (Gao et al., 2014; Singh et al., 2020; Wang-Erlandsson et al.,
86 2016). Our use of S_r is grounded in its effectiveness in representing ecosystems' access to soil moisture and their
87 ability to modify above-ground structures accordingly (de Boer-Euser et al., 2016; Singh et al., 2020; Stocker et
88 al., 2023; Wang-Erlandsson et al., 2016). It should be noted that we refer to rainforest tipping as a forest-savanna
89 transition 'risk' since the timing of such transitions depends on the stochastic fluctuations of other environmental
90 factors, beyond just hydroclimate (e.g., fire, human influence, species composition) (Cole et al., 2014; Cooper et
91 al., 2020; Higgins and Scheiter, 2012; Poorter et al., 2016). Therefore, to project if an ecosystem is a forest or
92 has tipped to savanna in the future, we assume the hydroclimate projected by the end of the 21st century (i.e.,
93 2086-2100) and ecosystem are in equilibrium. However, we do not account for the time required for ecosystems
94 to reach their (long-term) equilibrium state, which previous studies suggest can take between 50-200 years after
95 crossing the tipping point (Armstrong McKay et al., 2022).

96

97 **2 Methodology**

98 **2.1 Study Area**

99 This study focuses on forest ecosystems (i.e., excluding savanna/grassland and vegetation in human-influenced
100 ecosystems) extending between 15°N–35°S for South America and Africa.

101

102 **2.2 Data**

103 This analysis uses both empirical and ESM-simulated datasets of precipitation and evaporation. Empirical
104 datasets include remotely sensed and observation-corrected precipitation and evaporation time-series. Empirical
105 precipitation estimates at daily timestep are obtained from the Climate Hazards Group InfraRed Precipitation

106 with Station data (CHIRPS; 0.25° resolution) (Funk et al., 2015). Furthermore, empirical evaporation is derived
107 using an equally-weighted ensemble of three different datasets – (i) Breathing Earth System Simulator (BESS;
108 0.5° resolution) (Jiang and Ryu, 2016) (ii) Penman-Monteith-Leuning (PML; 0.5° resolution) (Zhang et al., 2016)
109 and (iii) FLUXCOM-RS (0.083° resolution) (Jung et al., 2019) - at monthly timestep. Here, evaporation
110 represents the sum of all evaporated moisture from the soil, open water and vegetation, including interception
111 and transpiration. We only selected evaporation datasets free from biome-dependent parameterisation (such as
112 plant function types, stomatal conductance, and maximum root allocation depth) and soil layer depth (represents
113 maximum depth of moisture uptake). Ultimately, all evaporation datasets are bilinearly interpolated to 0.25°
114 resolution and downscaled to daily timestep using ERA5 evaporation (0.25° resolution) estimates (Hersbach et
115 al., 2020). All empirical datasets are obtained for 2001-2012.

116 We also obtained precipitation and evaporation estimates from 33 ESMs (from 22 different institutes),
117 which includes CMIP6-historical and four SSP scenario simulations (SSP1-2.6 leads to approx. 1.3-2.4°C
118 warming; SSP2-4.5 corresponds to 2.1-3.5°C warming and is closest to the current trajectory according to the
119 nationally determined contributions (Anon, 2015); SSP3-7.0 around 2.8-4.6°C warming; and SSP5-8.5 represents
120 3.3-5.7°C warming; °C warming represents an increase in mean global surface temperature change by the end of
121 21st century relative to 1850-1900 (IPCC, 2021) (Fig. 1; Table S1 and S2). The historical estimates are obtained
122 at a monthly timestep for 2000-2014, and the estimates under different SSPs are obtained for 2086-2100. Though
123 obtained estimates from different ESMs are at different spatial resolutions, we bilinearly interpolated them to
124 0.25° for this analysis.

125 Finally, to minimise the influence of human activity and non-forest land cover on the natural water cycle,
126 we utilised land-cover data to remove pixels with such features from our analysis. We began by removing human-
127 influenced and non-forest land cover, such as savanna, grasslands, and water bodies, from Globcover, a global
128 land-cover classification dataset by the European Space Agency (ESA) at 300m resolution (GlobCover land-use
129 map, 2022). We then performed majority interpolation to convert the dataset to a 0.25° resolution and to mask
130 grid cells with less than 50% forest cover. This step ensured that only grid cells with over 50% forest cover were
131 classified as forests for further analysis.

132

133 **2.3 Root zone storage capacity-based framework for projecting forest transitions**

134 Vegetation uptakes soil moisture from its roots; thus, the availability of root zone moisture is a key element that
135 mediates the interaction between vegetation and climate (Brooks et al., 2015; Küçük et al., 2022; Rosas et al.,
136 2019; Wang-Erlandsson et al., 2022). However, measuring soil- (such as texture and porosity) and root-
137 characteristics (such as vertical and lateral extent and soil moisture uptake profiles) that influence access to
138 subsoil moisture are challenging to measure at ecosystem scales (Bruno et al., 2006). Furthermore, land-system
139 models tend to oversimplify the transfer and storage of water in root-zone due to insufficient knowledge about
140 soil-vegetation-climate interactions (Albasha et al., 2015; Hildebrandt et al., 2016; Wang et al., 2004). In such
141 cases, the mass-balance approach-based S_f provides a tangible and comprehensive understanding of ecosystem

142 access to moisture stored in the soil (de Boer-Euser et al., 2016; Gao et al., 2014; McCormick et al., 2021; Stocker
143 et al., 2023).

144

145 **2.3.1 Estimating mass-balance derived root zone storage capacity (S_r)**

146 Derived using the mass-balance approach, S_r represents the maximum amount of soil moisture accessed by
147 vegetation for transpiration (Singh et al., 2020; Wang-Erlandsson et al., 2016). This methodology calculates the
148 maximum extent of soil moisture within the reach of plant roots, assuming that ecosystems do not invest in
149 expanding their root-zone storage beyond what is necessary to bridge the maximum (accumulated) water-deficit
150 experienced by the vegetation during dry periods (i.e., periods in which evaporation is greater than rainfall,
151 irrespective of the seasons). This maximum annual accumulated water deficit ($D_{a,y}$) experienced by the ecosystem
152 is calculated using daily precipitation and evaporation estimates (Appendix A1 and Fig. A1). Subsoil moisture
153 beyond the reach of plant roots is primarily controlled by gravity-induced gradients (de Boer-Euser et al., 2016)
154 and is not available for transpiration. The rationale is that any extensive investment (i.e., more than necessary)
155 in root expansion would require carbon allocation and, thus, is inefficient from the perspective of the plants (Gao
156 et al., 2014; Schenk, 2008). Since this approach does not rely on prior information about vegetation, soil, or land
157 cover-based, by using empirical (observation-based) datasets (Appendix A1 and Fig. A1), we capture the
158 dynamics of actual soil moisture available for the ecosystems (Wang-Erlandsson et al., 2016). The detailed
159 methodology for calculating S_r using precipitation and evaporation estimates is outlined in Appendix A1.

160 In this mass-balance approach, S_r only represents a hydrological buffer essential for maintaining the
161 ecosystem's structure and functions (Gao et al., 2014; Wang-Erlandsson et al., 2016). However, other biotic and
162 abiotic factors, such as root morphology, soil depth, and geological formations, can physically restrict S_r by
163 limiting rooting depth, rooting structure, and the soil's water-holding capacity (Canadell et al., 1996; Jackson et
164 al., 1996; Schenk and Jackson, 2002) (Appendix A2). Additionally, soil properties like porosity or field capacity
165 could necessitate a deeper rooting strategy in different soil types (e.g., between sandy and clayey soil) to achieve
166 a comparable level of S_r to sustain the ecosystem under future climate (Kukul and Irmak, 2023). However, this
167 study assesses the impact of future climate change on the ecosystem's hydrological regime, focusing on the
168 changes to the ecosystem's equilibrium state. Therefore, the direct influence of soil and root characteristics under
169 future climate change on S_r (Appendix A2) and forest transitions falls outside our current scope.

170

171 **2.3.2 Determining root zone storage capacity thresholds for forest transitions**

172 A recent study by Singh et al. (2020) demonstrated that S_r can effectively represent an ecosystem's above-ground
173 state (i.e., whether it is a forest or savanna) and its level of water-stress, based on root-zone moisture availability.
174 In this study, we refine their terminology from 'water-stressed state' to 'water-limited state' to more precisely
175 describe the effects of changes in hydroclimatic conditions on forest and savanna ecosystems. They classified

176 these terrestrial ecosystem responses into four distinct categories based on the relationship between tree cover
177 density and root zone storage capacity (S_r) (for a more detailed description, see Singh et al., 2020):

- 178 i. **Lowly water-limited forest:** Dense forests (>70% tree cover) that receive ample rainfall (with daily
179 precipitation exceeding evaporation year-round; Singh et al., 2020) result in a very low $D_{a,y}$ (Appendix
180 A1). In such an environment, the top layer of the soil remains consistently damp, allowing for efficient
181 soil moisture uptake through shallow roots (<1m; S_r and maximum rooting depth comparison in Singh et
182 al., 2020), as vegetation typically utilises the shortest available pathway for moisture uptake (Bruno et
183 al., 2006). Consequently, these forest ecosystems can sustain themselves with a low S_r (<100 mm) (Singh
184 et al., 2020).
- 185 ii. **Moderately water-limited forest:** Although these forests retain a dense structure (>65% tree cover), the
186 increased precipitation seasonality (evaporation rates remain the same as before; Singh et al., 2020) leads
187 to a relatively higher $D_{a,y}$ (Appendix A1). This necessitates greater investment in their rooting systems
188 to access subsoil moisture for dry periods, with S_r for these ecosystems ranging between 100-400 mm in
189 South America and 100-350 mm in Africa (Singh et al., 2020). Notably, this enhanced below-ground
190 investment does not compromise the above-ground ecosystem structure, as evidenced by the changes in
191 ecosystem rooting structure relative to tree cover (Singh et al., 2020).
- 192 iii. **Highly water-limited forest:** With further increase in precipitation seasonality (even negligible
193 precipitation during dry seasons) and duration of dry period, forests need to maximise their S_r to sustain
194 their structure (see Fig. S2 and S3 in Singh et al., 2020). Maximum rooting depths of these ecosystems
195 can typically range between 15-20m (Singh et al., 2020). Maintaining ecosystems under these conditions
196 is costly from a subsoil investment perspective (Schenk, 2008), with regions in South America and Africa
197 showing S_r values as high as 750 mm and 450 mm, respectively (Singh et al., 2020). Consequently, these
198 values represent the upper limits beyond which forest ecosystems cannot further enhance their S_r (Singh
199 et al., 2020).

200 Possible mechanisms suggest that these trees adapt by shedding leaves to minimise moisture loss
201 (Wolfe et al., 2016). However, this adaptation can reduce photosynthetic activity, leading to declines in
202 root growth, and heightening the risk of mortality from hydraulic failures due to the unavailability of soil
203 moisture at accessible depths (Guswa, 2008). Furthermore, the accumulation of dry leaves also
204 perpetuates forest fires, thinning the ecosystem even further (tree cover can drop as low as 30%) (Nepstad
205 et al., 1999; Singh et al., 2020). Although increased tree mortality reduces competition for water, enabling
206 some trees to survive, the heightened risk of hydraulic failures and forest fires makes these ecosystems
207 highly susceptible to transitioning to savanna (Anderegg et al., 2016; Oliveras and Malhi, 2016; Sperry
208 and Love, 2015).

- 209 iv. **Savanna-grassland regime** (hereafter referred to as **savanna**): These ecosystems, typically
210 characterised by an open, grass-dominated structure (tree cover <40%), have both a lower water
211 availability and demand (both precipitation and evaporation are lower than in forest ecosystems) (Ratnam
212 et al., 2011; Singh et al., 2020). Thus, requiring a lower hydrological buffer to sustain their structure and

213 functions. For these ecosystems, S_r values can be as low as 100 mm (Singh et al., 2020). Although tree
214 species in this ecosystem can develop deep roots (extending up to 20m; see Fig. 2 and 3 in Singh et al.,
215 2020), the majority of the root biomass is concentrated in the shallow soil layers (top 30–50 cm; shallow
216 water uptake profile) (February and Higgins, 2010; Schenk, 2008). This strategy allows for competitive
217 moisture uptake between trees and grass species (Nippert and Holdo, 2015). This also suggests that, for
218 savanna, deeper roots don't always necessitate a high S_r (Singh et al., 2020).

219
220 The difference in S_r thresholds between both continents is due to the presence of water-use-efficient C4
221 grasses in Africa (Still et al., 2003), which reduces the competitiveness for moisture uptake between tree species
222 and grasses – leading to a lesser need for extensive S_r in the African forest ecosystem (Singh et al., 2020).
223 Furthermore, these adaptation dynamics align with the alternative stable state theory (i.e., forest's stabilising
224 feedback under hydroclimatic changes and tipping risk beyond certain hydroclimatic extremes) (Hirota et al.,
225 2011), which makes S_r more representative of the transient state of the ecosystem than precipitation (Singh et al.,
226 2022). We, thus, use these mass-balance derived S_r thresholds to project rainforest transitions and tipping risk
227 under future climate change. A detailed description of how previous studies have projected rainforest tipping
228 (Table S3), and how S_r -based framework builds upon their shortcomings is mentioned in the Supplement.

229

230 2.3.3 Projecting forest transitions under future climate change

231 Due to the lack of appropriate metrics for vegetation structure (e.g., tree cover density, tree height, floristic
232 patterns) and the reliance on assumptions about future land-use change (i.e., prescribed rather than biophysically
233 simulated) in ESMs (Hurtt et al., 2020), we use hydroclimate from ESMs as a proxy to project forest transitions
234 under future climate conditions. Using this proxy, we assume that the hydroclimate projected for the end of the
235 21st century and the ecosystem are in equilibrium (Staal et al., 2020). We start by classifying forests under the
236 current climate following the approach by Singh et al. (2020), which uses the (empirical) daily estimates of
237 CHIRPS precipitation and ensemble evaporation (2001-2012) (Appendix A1 and Sect. 2.3.2) (Fig. 1a). Since we
238 are only interested in forest transitions, the ecosystems classified as savanna under the current climate are
239 excluded from this analysis.

240 Next, for classifying ecosystems under future climate scenarios (Fig. 1b), we follow the same mass-balance
241 approach (Appendix A1). However, since precipitation and evaporation estimates from ESMs do not align with
242 empirical estimates (Baker et al., 2021; McFarlane, 2011), we employ a bias-correction method. Specifically, we
243 use a histogram equivalence method (Piani et al., 2010) to adjust empirical S_r thresholds to comparable CMIP6
244 S_r thresholds for various ESMs (Table S1). This involves, first, calculating S_r using CMIP6-historical
245 precipitation and evaporation estimates between 2000-2014 (Appendix A1 and Fig. S8). We then determine
246 percentile-equivalent S_r thresholds for each of the thirty-three CMIP6-ESMs under the current climate. For
247 example, if an empirical S_r of 100 mm corresponds to the 10th percentile ($n = 20\%$ of total pixels), we find the
248 10th percentile in the CMIP6-historically S_r , which may be higher or lower than 100 mm for each ESM (Fig. 1

249 and Table S1). These percentile-equivalent S_r thresholds are then used to classify ecosystems both under current
250 (CMIP6-historical; 2000-2014) and future climate (CMIP6-SSPs; 2086-2100) (Fig. 1b).

251 Ultimately, we evaluate potential transitions by comparing ecosystems classified under current climate
252 conditions (*this excludes savanna*) with those under future climate conditions (*this includes savanna*) (Sect.
253 2.3.2). These transitions are divided into three distinct categories (Fig. 1c and Fig. A2):

- 254 i. **Forest-savanna transition:** This refers to current climate forest ecosystems that risk transitioning to a
255 savanna under future climate change. To classify savanna under future climate conditions, we assume
256 the ecosystem is in equilibrium with the projected climate (see detailed steps in Appendix A3).
- 257 ii. **Transition to a more water-limited state:** This includes ecosystems that shift to a higher water-limited
258 state in the future. For example, if a forest currently classified as lowly water-limited transitions to either
259 a moderately or highly water-limited state in the future, it would fall under this category.
- 260 iii. **Reversion to a less water-limited state:** This includes ecosystems that shift to a lower water-limited
261 state in the future.

262

263 To aggregate the results from all ESMs, grid cells with $> 50\%$ convergence are referred to as ‘moderate-
264 high model agreement’, 20-50% as ‘moderate model agreement’ and $\leq 20\%$ as ‘low model agreement’. In the
265 Results section, we primarily discuss estimates from scenarios $>20\%$ and $>50\%$ model convergence. While a
266 threshold of $>20\%$ may seem low given the total number of ESMs analysed, it is important to recognise the
267 variable and often limited capabilities of these ESMs, particularly in simulating biophysical interaction and
268 emerging properties due to our limited understanding of the Earth system (Lenton et al., 2019; Stevens and Bony,
269 2013). Opting for a majority-based consensus in ESMs could overlook critical tipping risks identified by a
270 minority of models, which might provide insights as valid as those from more widely agreeing models (Arora et
271 al., 2023; Reyer et al., 2015).

272

273 2.4 Sensitivity analyses

274 Our methodology operates under two key assumptions: (i) the empirically derived S_r thresholds remain valid in
275 the future, and (ii) the hydroclimatic estimates projected by ESMs accurately represent the actual climate, even
276 though these models have prescribed land cover (Hurtt et al., 2020). To address the uncertainties related to the
277 first assumption, we conduct four sensitivity analyses to assess the robustness of our analysis: (a) assuming that
278 the regions exceeding the 99th percentile S_r are prone to a forest-savanna transition, as high S_r investment could
279 be unrealistic from the perspective of plants under future climate change, (b) evaluating forest transitions using
280 three different evaporation datasets, (c) assessing forest transitions under 10- and 40-year drought return periods,
281 and (d) adjusting the forest-savanna transition thresholds.

282 Regarding the second assumption, we explicitly apply this methodology across a wide range of available
283 ESMs under four SSP scenarios to identify consistencies and discrepancies in the results. Additionally, the

284 discrepancies between the prescribed land use and the forest transitions derived from our methodology, as well
285 as the implications of these assumptions, are detailed in the Discussion section.

286

287 **3 Results**

288 We find that under future climate conditions (2086-2100), considering >50% models' agreement, about one-
289 fourth of the forests in both South America and Africa are projected to transition (Fig. 2b-g). With >20% models'
290 agreement, these transitions are projected to occur for about three-fourths of the forests for both continents.
291 Considering a lower threshold for models' agreement causes double or triple counting of some transitions (Fig.
292 2b-g). To minimise this in further analyses, we only consider >50% models' agreement for forests that transition
293 to a more and less water-limited state. Furthermore, because (abrupt) forest-savanna transitions are under-
294 represented in ESMs (Drijfhout et al., 2015; Lenton, 2011; Maslin and Austin, 2012; Valdes, 2011), we consider
295 >20% models' agreement for them. Considering this, we not only reduce the overlap to <0.4% of the total forest
296 area (Fig. S9), but we also maximise highlighting forest-savanna transition risk for both continents.

297 We find that the risk of forest-savanna transitions mainly occurs in the Guiana Shield of South America,
298 and the southern and south-eastern regions of Africa (Fig. 3). Compared to Africa, forest-savanna transitions are
299 more prominent in South America under warmer climates (i.e., higher SSPs; Fig. 2b and 3). Our analysis reveals
300 that the extent of forest-savanna transitions in South America decreases from almost $1.32 \times 10^6 \text{ km}^2$ (16.3% of
301 total forest area in South America) under the highest emission scenario to $0.04 \times 10^6 \text{ km}^2$ (0.5%) under the lowest
302 emission scenario (Fig. 2b). Interestingly, for Africa, the extent of forest-savanna transition did not change much
303 for different SSPs, i.e., (median) $0.25 \times 10^6 \text{ km}^2$ with a maximum deviation of $\pm 0.11 \times 10^6 \text{ km}^2$ (minimum and
304 maximum extent of transition between 3-6.6% of total forest area in Africa) (Fig. 2c).

305 When comparing the changes in forest-savanna transition risk areas relative to their immediate lower
306 warming scenarios, we find considerable increases for South America. The highest relative growth of
307 approximately 5.75 times is observed between SSP1 and SSP2, with the forest area under risk increasing from
308 $0.04 \times 10^6 \text{ km}^2$ to $0.23 \times 10^6 \text{ km}^2$, respectively. It increases by 3.48 times from SSP2 to SSP3 ($0.23 \times 10^6 \text{ km}^2$ to
309 $0.80 \times 10^6 \text{ km}^2$), and by 1.65 times from SSP3 to SSP5 ($0.80 \times 10^6 \text{ km}^2$ to $1.32 \times 10^6 \text{ km}^2$). For Africa, however,
310 the increases are more modest: the risk grows by 1.29 times from SSP1 to SSP2 ($0.17 \times 10^6 \text{ km}^2$ to 0.22×10^6
311 km^2), by 1.63 times from SSP2 to SSP3 ($0.22 \times 10^6 \text{ km}^2$ to $0.36 \times 10^6 \text{ km}^2$), and is observed to decrease by 0.72
312 times from SSP3 to SSP5 ($0.36 \times 10^6 \text{ km}^2$ to $0.26 \times 10^6 \text{ km}^2$).

313 By evaluating changes to their hydroclimate, we find that under warmer climates, forest-savanna transition
314 regions in both continents are projected to experience a decrease in precipitation. Furthermore, we observe an
315 increase in precipitation seasonality for South America, whereas Africa shows a decrease (Fig. S12). Here, an
316 increase in precipitation seasonality (seasonal variability in precipitation over the year) creates water-limited
317 conditions for the ecosystem. In contrast, a decrease in seasonality and precipitation in Africa corresponds to a
318 lower moisture availability altogether. Nevertheless, for both these continents, this transition seems to occur for
319 the previously highly water-limited forests under the current climate, followed by moderately, with the least

320 contribution from lowly water-limited forests (Fig. 3). This highlights the looming risk on highly water-limited
321 forests to experience a forest-savanna transition under warmer climates.

322 Forests that transition to a ‘more’ water-limited state in South America are spatially aggregated towards
323 the border between Brazil, Colombia, and Peru – covering a considerable portion of the Central Amazon (Fig.
324 3). Whereas for Africa, these forests exist in moderate to small patches towards the northern and southern extent
325 of central Congo rainforests. We observe that these transitions account for most of the projected changes to
326 forests’ states across both continents (Fig. 2d,e), with the transition to just the ‘highly water-limited forest’
327 accounting for more than three-fourths of all such transitions (Fig. 3). We observe that South American forests
328 gradually become increasingly water-limited under warmer climates, with maximum and minimum projected
329 transition of $1.89 \times 10^6 \text{ km}^2$ (23.4%) and $1.61 \times 10^6 \text{ km}^2$ (19.9%) observed under the highest and lowest emission
330 scenarios, respectively (Fig. 2d,e). Whereas for Africa, the change in the water-limited state of the forests under
331 different SSP scenarios remains almost similar (i.e., median $1.14 (\pm 0.06) \times 10^6 \text{ km}^2$; 19.6-22.2%). Analysis of
332 their hydroclimatic changes reveals that water-limitation is induced by both a decrease in precipitation and an
333 increase in seasonality in South America (Fig. S13). In contrast, water-limitation in Africa is driven solely by an
334 increase in seasonality. We observe that these newly water-limited forests seem to have permeated to regions that
335 were previously (under the current climate) dominated by lowly and moderately water-limited forests (Fig. 3).
336 Here, this shift only signifies the changes to hydroclimatic conditions allowing forests to transition to a more
337 water-limited state, rather than the changes to the floristic composition of terrestrial species from one location to
338 another. Although such a shift under changing climate is not unlikely (Esquivel-Muelbert et al., 2019), they are
339 not analysed in this study.

340 Forests that revert to a ‘less’ water-limited state in South America are primarily observed in the south-
341 eastern Amazon, with small patches observed towards eastern Brazil and the western coast of Equatorial Guinea
342 and Gabon (Fig. 3). For Africa, the reverted forests exist in patches in the northern and southern regions of the
343 Congo rainforest. Furthermore, for South America, we observe a gradual decrease in these reversions with an
344 increase in warming. Here, we observe the lowest reversion of $0.23 \times 10^6 \text{ km}^2$ (2.8%) under the highest emission
345 scenario and the highest reversion of $0.67 \times 10^6 \text{ km}^2$ (8.4%) under the lowest emission scenario (Fig. 2f,g). For
346 Africa, these trends remain almost similar under all SSPs (i.e., median $0.18 (\pm 0.05) \times 10^6 \text{ km}^2$; 2.2-3.5%).
347 Comparing these transitions with their hydroclimatic changes reveals an overall increase in precipitation (Fig.
348 S14). Interestingly, we observe a much higher precipitation increase for South America under high-emission
349 scenarios than those in lower-emission scenarios. However, we find that precipitation seasonality is also higher
350 for these ecosystems under warmer climates (Fig. S14). This suggests that increased precipitation without
351 changes to precipitation seasonality helps decrease the water-limitation of the ecosystem, compared to the
352 ecosystems that experienced a simultaneous increase in both.

353 Our sensitivity analysis, detailed in Appendix B1, reveals a consistent pattern of forest transitions across
354 various scenarios.

355
356

357 4 Discussion

358 4.1 Asynchronous resilience risks under future climate change

359 Our analysis reveals the spatial extent of potential ecosystem transitions in South America and Africa and their
360 vulnerability to future climate change (Fig. 2 and 4). For South America, we find a clear indication of a decrease
361 in forest resilience (i.e., an increase in water-limited forests) and an increase in forest-savanna transition risk
362 under warmer climates (Fig. 2b,d,f). In contrast, these trends are not symmetric for Africa, where transition risk
363 shows only slight variation across the different SSPs (Fig. 2c,e,g). Similar to the results of this study, previous
364 studies on rainforest tipping have also suggested that exceeding 1.5-2°C will considerably increase the tipping
365 risk (Flores et al., 2024; Jones et al., 2009; Parry et al., 2022), with the Guyana Shield in the Amazon being the
366 most susceptible under future climate change (Cox et al., 2004; Staal et al., 2020) (Fig. 3 and Table S3). Previous
367 studies also agree that, in contrast to the Amazon, the projected risk to Congo rainforests is not substantial
368 (Higgins and Scheiter, 2012; Staal et al., 2020) (Fig. 2). Despite it being unclear to what extent the ESMs
369 represent the correct carbon-water dynamics (Koch et al., 2021), our results show a further divergence between
370 Amazon's and Congo's responses to different SSPs (Fig. 2 and Fig. S12-S14). This could either be caused simply
371 by a different response to changes in precipitation patterns over the respective regions (Kooperman et al., 2018;
372 Li et al., 2022) or a different response to increased CO₂ levels in the atmosphere (Brienen et al., 2015; Hubau et
373 al., 2020; Trumbore et al., 2015).

374 Previous empirical studies have linked these divergent responses to evolutionary and biogeographical
375 differences between the ecosystems, which resulted in distinct species pools that uniquely influence each
376 ecosystem's adaptability and response to climate change (Fleischer et al., 2019; Hahm et al., 2019; Hubau et al.,
377 2020; Slik et al., 2018). These studies found that forest ecosystems in the Amazon tend to be more dynamic –
378 grow faster due to high CO₂ levels in the atmosphere – than those in the Congo rainforests. However, these fast-
379 growing trees also die young due to them investing substantially less in their adaptive strategies against
380 perturbations than (less dynamic) old-growth forests (Brienen et al., 2015; Körner, 2017; Rammig, 2020). This
381 makes the Amazon rainforest especially sensitive to CO₂ emissions pathways, as the positive influence of CO₂
382 fertilisation-induced growth is counteracted by the negative impact of warming and droughts, thereby
383 exacerbating the risk of forest mortality under high emission scenarios (Brienen et al., 2015; Hubau et al., 2020;
384 Yang et al., 2018). In this case, the projected changes to the future hydroclimate could be an artefact of decreased
385 transpiration and precipitation due to forest mortality, rendering the rainforests vulnerable to tipping. In contrast,
386 terrestrial species in Congo rainforests appear more resilient, having adapted to severe droughts during glacial
387 periods, which makes them better equipped to handle episodic water-induced perturbations than Amazon (Cole
388 et al., 2014).

389 Nevertheless, with compounding influence from land-use and climate-induced hydroclimatic changes
390 (Davidson et al., 2012), these rainforests risk tipping to a savanna state. Our results highlight that by keeping the
391 mean global surface temperature below 1.5-2°C warming (which in this case is equivalent to SSP1-2.6 relative

392 to the pre-industrial), we minimise forest-savanna transition risk and maximise recovery – thereby improving the
393 resilience of rainforest ecosystems (Fig. 2, 3 and 4).

394

395 **4.2 Changes in atmospheric moisture flow drives forest-savanna transition**

396 Among all transitions, the most noticeable and catastrophic (since it is difficult to revert) is the forest-savanna
397 transition projected in the Amazon’s Guiana Shield of South America, and over the southern and south-eastern
398 parts of Africa (Fig. 3 and 4). These transitions are associated with the shifting of the inter-tropical convergence
399 zone (ITCZ) (Mamalakis et al., 2021), which decreases precipitation and increases precipitation seasonality over
400 the continents. For South America, the creation of these low-pressure bands allows the trade winds to bring in
401 considerable moisture from the equatorial Atlantic Ocean over to Amazon by passing through the Guiana Shield
402 and ultimately carrying it across the La Plata Basin via the South American low-level jet (Bovolo et al., 2018;
403 van der Ent et al., 2010; Zemp et al., 2014). Similarly, for Africa, south-eastern trade winds bring moisture from
404 the Indian Ocean over the centre of the African continent (Mamalakis et al., 2021).

405 Under a warmer climate, sea surface temperature over the equatorial Atlantic and the northern Indian
406 Ocean is projected to increase (Pascale et al., 2019; Zilli et al., 2019), leading to a southward shift in ITCZ over
407 the eastern Pacific and Atlantic Oceans, and northward over east Africa and the Indian Ocean (Mamalakis et al.,
408 2021; Xie et al., 2010). Previous studies also acknowledge that the intense surface warming over the Sahara under
409 future climate can also attract ITCZ northwards in Africa (Cook and Vizzy, 2012; Dunning et al., 2018; Mamalakis
410 et al., 2021). These climate change-induced shifts in ITCZ can potentially both mitigate and exacerbate the effects
411 of (accumulated) water-deficit on the forest ecosystem, especially critical for highly water-limited forests, even
412 without considering the changes to atmospheric moisture flow caused by localised deforestation (Leite-Filho et
413 al., 2021; Schumacher et al., 2022; Staal et al., 2018; Wunderling et al., 2022). This underscores the importance
414 of including changes in atmospheric circulation in studies that analyse the impact of future climate on the
415 resilience of forest ecosystems (Staal et al., 2020; Zemp et al., 2017).

416

417

418 **4.3 Discrepancy between prescribed future land use and projected transitions**

419 The land-use information in CMIP6-ESMs is not biophysically simulated, but prescribed based on simulations
420 from Integrated Assessment Models (IAMs) for each SSP scenario (Hurtt et al., 2020). Therefore, it is valuable
421 to examine whether these prescribed land-use scenarios agree or conflict with the changes projected (assuming
422 equilibrium between hydroclimate and the ecosystem) by our S_r -based ecosystem transitions (Fig. 5 and Fig. S15-
423 S17).

424 The most noticeable discrepancies are observed in South America, where the extent of forest-savanna
425 transitions is underestimated in prescribed land-use scenarios compared to those projected in this study (i.e.,
426 prescribed land-use predicts forests in the region whose hydroclimate can’t support forest; Fig. 4 and 5a).
427 Additionally, in South America, our analysis highlights the potential of some forests reverting to a ‘less water-

428 limited state' in places where the prescribed land use in the ESMs suggests non-forest landscapes (Fig. 4 and 5c).
429 These discrepancies arise because the prescribed land use in CMIP6-ESMs does not shift in response to
430 hydroclimatic changes. Despite our approach assuming equilibrium and overlooking the temporal dynamics of
431 transitions, based on broad climate change patterns (Sect 4.2), we believe it more accurately represents the
432 ecohydrological state of the ecosystems.

433 However, these prescribed land uses can introduce errors in subsequent biophysical processes simulated
434 in ESMs (Ma et al., 2020), affecting the accuracy of projected transitions. For example, prescribing a region as a
435 forest that would be grassland in the future will lead to the extraction of deeper subsoil moisture in ESMs, which
436 (actual) grasslands do not have the capacity to access (Ahlström et al., 2017; Yu et al., 2022). This will result in
437 an overestimation of the ecosystem's evaporation, potentially altering precipitation patterns downwind and
438 leading to inaccurate water budget assessments for these ecosystems. Consequently, causing erroneous
439 projections of the ecosystem state. These discrepancies underscore the urgent need for enhancements in the land
440 surface components of ESMs, enabling dynamic simulations of vegetation-climate feedbacks. Such
441 improvements would provide a more accurate representation of the ecohydrology of terrestrial ecosystems and
442 their response to changing climate conditions.

443

444 **4.4 Limitations**

445 This study assumes that the S_r -derived thresholds used to classify terrestrial ecosystems under current climate
446 conditions remain valid under future climate change. However, forests themselves are dynamically adapting their
447 structure and functions in response to climate change, altering their critical thresholds (Doughty et al., 2023).
448 Thus, assuming a static critical threshold may lead to inaccuracies in estimating forests' resilience to future
449 climate change. For instance, under the CO₂ fertilisation effect, forests may become more water-use efficient
450 (i.e., transpire less and therefore need for a lower S_r) (Xue et al., 2015), potentially delaying their tipping under
451 warming scenarios compared to those projected in this study. Conversely, factors such as nutrient limitation
452 (Condit et al., 2013) or extensive human influence (van Nes et al., 2016) in the ecosystem might lead to an earlier
453 tipping than anticipated.

454 However, the uncertainty surrounding the effect of CO₂ fertilisation, nutrient limitation, and human
455 influence on vegetation remain significant research frontiers for enhancing our understanding of rainforest tipping
456 under future climate change (Fleischer et al., 2019; Hofhansl et al., 2016). Additionally, factors such as
457 precipitation variability, species composition, soil properties, and topography can contribute to varied local-scale
458 forest responses to future climate change (Staal et al., 2020). It should also be noted that though these
459 uncertainties may hinder our understanding of local-scale forest resilience, the influence of future hydroclimatic
460 changes on forests still constitutes major prediction uncertainties. Therefore, in this study, regardless of how
461 these influences are parametrised or simulated in each ESM, we assume that hydroclimatic estimates projected
462 by the ESMs represent the actual climate.

463 Of course, this assumption opens us and other studies projecting forest conditions to future climate
464 change to certain limitations. Our ability to project forest-savanna transitions (or any transition) relies on the
465 model's capacity to simulate complex feedbacks. Some models capture complex vegetation-atmosphere
466 interaction, simulating local and regional scale feedbacks across time (Ferreira et al., 2011; Jach et al., 2020);
467 others rely on simpler parametrisation (Nof, 2008) (e.g., parametrisation of CO₂ fertilisation; Koch et al., 2021).
468 However, caution should be taken to not overgeneralise the functioning of tropical forests just from the analysis
469 presented in this study, and also realise the current potential of ESMs to simulate them (Staal et al., 2020). We
470 believe that by considering simulations from multiple ESMs under different SSP scenarios, not only do we
471 highlight the agreements and conflicts between potential transitions; but also allow future studies to disentangle
472 vegetation-climate feedbacks and improve the modelling of local-scale interactions (e.g., vegetation's water-
473 uptake profile, species response to CO₂ fertilisation) in the ESMs.

474

475 **5 Conclusions**

476 Classifying terrestrial ecosystems based on empirical and CMIP6 ESMs-derived S_r allowed us to assess the future
477 transitions in the rainforest ecosystems. Our findings indicate that the climate projected under the lowest emission
478 scenarios significantly reduces the risk of rainforest tipping and maximises reversion to a less water-limited state,
479 while the climate projected under the high emission scenarios has the opposite effect on the forest ecosystem.
480 Specifically, in the Amazon rainforest, the risk of forest-to-savanna transition increases considerably with
481 incremental increases in warming. Conversely, in the Congo, the variation in transition risk across different
482 emission scenarios is relatively minor.

483 Notably, our analysis suggests a very limited tipping risk that is 'unavoidable' (i.e., regions prone to a
484 forest-savanna transition in all scenarios), and the vast majority of potential transition risks can still be avoided
485 by steering towards a less severe climate scenario, thereby underscoring the critical window of opportunity.
486 Moreover, regions projected to revert to a less water-limited state could potentially become more amenable to
487 restoration and responsive to deforestation prevention efforts. This study highlights the importance of restricting
488 global temperature change below 1.5-2°C warming relative to the pre-industrial levels to prevent forest tipping
489 risks and provide the best conditions for effective ecosystem stewardship.

490

491 **Appendix A: Methodology**

492 **A1. Root zone storage capacity calculation**

493 Our method to calculate S_r is adopted from Singh et al. (2020). For estimating S_r , we first obtained the water
494 deficit (D_t) at daily time step from the daily estimates of precipitation (P_t) and evaporation (E_t) (Fig. A1) using:

$$495 \quad D_t = E_t - P_t \quad (\text{A1})$$

496 Here, t denotes the day count since the start of the simulation, with simulation for each grid starting in
 497 the month with maximum precipitation. Second, we calculated the accumulated water deficit integrated at each
 498 one-day timestep for one year using:

$$499 \quad D_{a(t+1)} = \max\{0, D_{a(t)} + D_{t+1}\} \quad (\text{A2})$$

500 Where $D_{a(t+1)}$ is the accumulated water deficit at each time step (Fig. A1). Here, an increase in the
 501 accumulated water deficit will occur when $E_t > P_t$, and a decrease when $E_t < P_t$. However, since this algorithm
 502 estimates a running estimate of root zone storage reservoir size, we use a maximum function to calculate the
 503 accumulated water deficit, which by definition can never be below zero. Not allowing $D_{a(t+1)}$ to be negative also
 504 means that excess moisture from precipitation will either contribute to deep drainage or runoff. Lastly, the
 505 maximum accumulated annual water deficit ($D_{a,y}$) will represent the maximum storage required by the vegetation
 506 to respond to the critical dry periods (Fig. A1).

$$507 \quad D_{a,y} = \max\{D_{a(t+1)}\} \quad t = 1 : n - 1 \quad (\text{A3})$$

508 This simulation runs for a whole year, with n denoting the number of days in year y .

509 Different terrestrial ecosystems (e.g., forest, savanna and grassland) adapt to different drought return
 510 periods (de Boer-Euser et al., 2016; Gao et al., 2014; Wang-Erlandsson et al., 2016). For instance, grasslands and
 511 savannas adapt to shorter drought return periods (i.e., <10 years and 10-20 years, respectively). In contrast, forests
 512 adapt to long drought return periods (>40 years) (Wang-Erlandsson et al., 2016). For this study, we use a uniform
 513 20-year drought return period (following Bouaziz et al., 2020; Nijzink et al., 2016) to avoid any artificially
 514 introduced transitions between different ecosystems. Thus, this 20-year drought return period S_r refers to the
 515 maximum amount of root zone moisture accessible to vegetation for transpiration during the largest accumulated
 516 annual water deficit expected every twenty years under static climate conditions. We analyse this using the
 517 Gumbel extreme value distribution (Gumbel, 1958) and apply it to normalise all $D_{a,y}$. The Gumbel distribution
 518 ($F(x)$) is given by:

$$519 \quad F(x) = \exp\left[-\exp\left[-\frac{(x - \mu)}{\alpha}\right]\right] \quad (\text{A4})$$

520 Where μ and α are the location and scale parameters, respectively. We calculate this using the python
 521 package 'skextremes'(skextremes Documentation):

$$522 \quad S_r = \overline{D_{a,y}} + K \times \sigma_{n-1} \quad (\text{A5})$$

523 Where K is the frequency factor given by:

$$524 \quad K = \frac{y_t - y_n}{S_n} \quad (\text{A6})$$

525 And y_t is the reduced variate given by:

526

$$y_t = - \left[\ln \left[\ln \left(\frac{T}{T-1} \right) \right] \right] \quad (\text{A7})$$

527

528

529

530

531

Where T is the drought return period (i.e., 20 years used in this study), $\overline{D_{a,y}}$ is the mean annual accumulated deficit for the years 2001-2012, σ_{n-1} is the standard deviation of the sample. Also, \mathcal{Y}_n is the reduced mean and S_n is the reduced standard deviation, which for $n = 11$ years (since we are calculating S_r in a hydrological year – simulation starts mid-year – we therefore lose one year) is equal to 0.4996 and 0.9676, respectively (Gumbel, 1958).

532

533

534

Since the CMIP6 (-historical and -SSP estimates, the timeframe considered are 2000-2014 and 2086-2100, respectively) doesn't have daily estimates of evaporation and precipitation for all Earth System Models (ESMs), we directly use the monthly estimates of precipitation and evaporation to modify Eq. (A1) as:

535

$$D_t = E_{t(\text{monthly})} - P_{t(\text{monthly})} \quad (\text{A8})$$

536

537

538

539

Here, $t(\text{monthly})$ denotes the month count since the start of the simulation. The rest of the steps (Eq. A2-A7) remain the same for CMIP6 datasets. For CMIP6 runs, \mathcal{Y}_n and S_n in Eq. (6) are calculated for $n = 14$ years (Eq. A7) equal to 0.5100 and 1.0095, respectively. The S_r estimates derived from daily and monthly empirical estimates (from Eq. A1 and A8) are compared in Fig. S8 to evaluate uncertainty.

540

541

A2. Abiotic and biotic factors influence soil moisture availability

542

543

544

545

546

547

548

In this study, S_r quantifies the hydrological buffer necessary for an ecosystem to maintain its structure and functions, reflecting the amount of root zone soil moisture available to vegetation for transpiration. Our mass-balance-based S_r methodology, while not directly distinguishing between the biotic and abiotic influences on soil moisture and root characteristics, does incorporate their critical role in shaping the ecohydrology of the ecosystem under climate change. By utilising empirical precipitation and evaporation data, our approach theoretically captures the combined impact of these biotic and abiotic factors on the actual hydrological regime (including soil moisture) of the ecosystem (Sect. 2.3.2).

549

550

551

552

553

554

555

556

We acknowledge that abiotic factors such as soil texture, structure, and depth profoundly affect soil water-holding capacity (Fayos, 1997). For instance, field studies suggest that clay and organic-rich soils exhibit superior water retention capabilities due to their fine textures and high surface areas, crucial to vegetation for moisture uptake during extended dry periods (Bronick and Lal, 2005; Fayos, 1997). Additionally, the depth and porosity of soil also dictate its ability to absorb and store water in the soil, with deeper, less compacted soils providing a higher buffer against drought by allowing greater water infiltration (Indoria et al., 2020; Smith et al., 2001). By altering temperature and precipitation patterns, climate change can modify these abiotic soil properties, potentially leading to a loss in soil water retention capacity through erosion and compaction (Dexter, 2004).

557 Moreover, biotic factors, including plant-root dynamics and microbial activity, also play essential roles
558 in shaping the ecosystem (Brunner et al., 2015; Sveen et al., 2024). Deep and extensive root systems not only
559 directly improve access to deeper soil moisture, but also physically modify the soil to enhance its permeability
560 and storage (Canadell et al., 1996; Jackson et al., 1996). Additionally, microbial processes contribute by breaking
561 down organic matter, thereby improving the soil's structural integrity and ability to retain water (Dittert et al.,
562 2006). These biotic interactions, coupled with changing abiotic factors under climate change, underscore the
563 complex dynamics that govern soil moisture availability and ecosystem resilience. However, this study does not
564 consider the direct impact of future climate change on biotic and abiotic factors, nor their influence on
565 ecosystems, beyond changes to S_r .

566

567 **A3. Using precipitation to discern savanna from forests under future climate change**

568 Under future climate change, some ecosystems will remain forest, while others may transition to savanna.
569 In our S_r -based framework, without information about above-ground forest structure, it is difficult to discern
570 whether an ecosystem is a forest or savanna just with S_r (for instance, an ecosystem with S_r of 200 mm can either
571 be a moderately water-limited forest or savanna; Sect. 2.3.2). Differentiating these ecosystems is easier under the
572 current climate, where we have several remote sensing products capturing vegetation structure (e.g., tree cover
573 density, tree height, floristic patterns) (Aleman et al., 2020; Hirota et al., 2011; Xu et al., 2016). However, under
574 future climate, we must find a proxy, since land-use information in ESMs is prescribed (i.e., not biophysically
575 simulated) (Ma et al., 2020).

576 To address this, previous studies have either relied on vegetation structure proxies provided by ESMs (e.g.,
577 net primary productivity) (Boulton et al., 2013; Jones et al., 2009) or assumed that terrestrial ecosystems are in
578 equilibrium with their climate (Staal et al., 2020) (see Supplement). In this study, we adopted the latter approach
579 and utilised climate variables, specifically (bias-corrected) mean annual precipitation and the precipitation
580 seasonality index, as proxies to make this distinction (Fig. S4). The climate conditions (or range) necessary for
581 forest ecosystems to sustain themselves are determined by comparing empirical estimates of mean annual
582 precipitation and precipitation seasonality index with S_r . These estimates are then bias-corrected (following the
583 same methods described in Sect. 2.3.3) before applying them to future climate scenarios. This (revised)
584 classification of terrestrial ecosystems is then used to assess forest transitions under future climate change
585 scenarios.

586

587 **Appendix B: Results**

588 **B1. Sensitivity analysis reveals robust performance of the framework**

589 Sensitivity analysis reveals that by setting an extreme S_r threshold – signifying a forest-savanna transition for
590 ecosystems that cannot maintain their above-ground structure at high S_r – we observe some shifts near the already
591 projected risk regions and coastal areas (Fig. 3 and Fig. S18). However, the transition risk identified in the coastal

592 regions may be an artefact of interpolating hydroclimate estimates to higher resolution. Additionally, since
593 evaporation is more prevalent over oceans than land, this could result in high S_r values, thereby projecting an
594 elevated tipping risk in these coastal areas.

595 We also discover that variations in the evaporation datasets and return periods used for calculating S_r
596 have minimal effect on forest transitions (Fig. S19 and S20). Although the forest classification thresholds may
597 shift with different evaporation products under current climate conditions (Singh et al., 2020), our histogram
598 equivalence method ensures that forest classifications under future climates adjust accordingly, resulting in only
599 minor alterations to the final outcome (Fig. 1b and Fig. S19). Furthermore, while S_r values tend to increase with
600 increase with shorter return periods, the impact of these changes becomes less significant with longer return
601 periods (Wang-Erlandsson et al., 2016), leading to minor variations in the end results (Fig. S20).

602 Moreover, lowering the forest-savanna transition thresholds can reduce the risk of forest-savanna
603 transition since it expands the associated range of climate conditions (i.e., mean annual precipitation and
604 seasonality) necessary for forests to sustain their structure and functions (Fig. S21). Conversely, increasing the
605 forest-savanna transition threshold leads to an opposite trend, where the risk of transition increases (Fig. S22).
606 Despite these sensitivity analyses, the variation in transition magnitudes is minor, and the trends across different
607 SSP scenarios for both continents remain consistent (Fig. 2 and Fig. S18-S22). Therefore, the conclusions drawn
608 from this study remain robust, even with variations in factors that could potentially affect forest transitions.

609 **Code availability**

610 The python-language scripts used for the analyses presented in this study are available from GitHub:
611 <https://github.com/chandrakant6492/Future-forest-transitions-CMIP6>. The python-language code for
612 calculating (empirical) root zone storage capacity is available from GitHub:
613 <https://github.com/chandrakant6492/Drought-coping-strategy>.

614 **Data availability**

615 All the data generated during this study is made publicly available at Zenodo:
616 <https://zenodo.org/record/7706640>. Other datasets that support the findings of this study are publicly available
617 at: (CMIP6; citations referred to in Table S2) <https://aims2.llnl.gov/>, (Root zone storage capacity; empirical)
618 <https://github.com/chandrakant6492/Drought-coping-strategy>, (P-CHIRPS)
619 <https://data.chc.ucsb.edu/products/CHIRPS-2.0/>, (E-BESS) <ftp://147.46.64.183/>, (E-FLUXCOM) [ftp.bgc-](ftp.bgc-jena.mpg.de)
620 [jena.mpg.de](ftp.bgc-jena.mpg.de), (E-PML) <https://data.csiro.au/collections/#collection/Cicsiro:17375v2>, (E-ERA5)
621 <https://cds.climate.copernicus.eu/cdsapp#!/dataset/reanalysis-era5-single-levels>, (Globcover)
622 http://due.esrin.esa.int/page_globcover.php. Potential transitions for each ESM based on the comparison
623 between empirical (2001-2012) and SSP (2086-2100) scenarios are presented in the Supplement.

624 **Author contribution**

625 All authors contributed to the conceptualisation of this research. CS performed the analyses and wrote the initial
626 draft. All authors contributed to the discussion and revisions, leading to the final version of the manuscript.

627 **Competing interests**

628 The authors declare that they have no conflict of interest.

629 **Acknowledgements**

630 C.S., I.F. and L.W.-E. acknowledge funding support from the European Research Council (ERC) project ‘Earth
631 Resilience in the Anthropocene’, project number ERC-2016-ADG-743080. L.W.-E. also acknowledges funding
632 support from the Swedish Research Council for Sustainable Development (FORMAS), project number 2019-
633 01220 and the IKEA Foundation. R.v.d.E. acknowledges funding support from the Netherlands Organisation for
634 Scientific Research (NWO), project number 016.Veni.181.015. The authors also acknowledge the computational
635 support provided by Microsoft Planetary Computer (<https://planetarycomputer.microsoft.com>) for performing
636 the analyses.

637

638

639 **References**

- 640 Ahlström, A., Canadell, J. G., Schurgers, G., Wu, M., Berry, J. A., Guan, K., and Jackson, R. B.: Hydrologic
641 resilience and Amazon productivity, *Nature Communications*, 8, 387, [https://doi.org/10.1038/s41467-017-](https://doi.org/10.1038/s41467-017-00306-z)
642 00306-z, 2017.
- 643 Albasha, R., Mailhol, J.-C., and Cheviron, B.: Compensatory uptake functions in empirical macroscopic root
644 water uptake models – Experimental and numerical analysis, *Agricultural Water Management*, 155, 22–39,
645 <https://doi.org/10.1016/j.agwat.2015.03.010>, 2015.
- 646 Aleman, J. C., Fayolle, A., Favier, C., Staver, A. C., Dexter, K. G., Ryan, C. M., Azihou, A. F., Bauman, D.,
647 Beest, M. te, Chidumayo, E. N., Comiskey, J. A., Cromsigt, J. P. G. M., Dessard, H., Doucet, J.-L., Finckh, M.,
648 Gillet, J.-F., Gourlet-Fleury, S., Hempson, G. P., Holdo, R. M., Kirunda, B., Kouame, F. N., Mahy, G.,
649 Gonçalves, F. M. P., McNicol, I., Quintano, P. N., Plumptre, A. J., Pritchard, R. C., Revermann, R., Schmitt, C.
650 B., Swemmer, A. M., Talila, H., Woollen, E., and Swaine, M. D.: Floristic evidence for alternative biome states
651 in tropical Africa, *PNAS*, 117, 28183–28190, <https://doi.org/10.1073/pnas.2011515117>, 2020.
- 652 Anderegg, W. R. L., Klein, T., Bartlett, M., Sack, L., Pellegrini, A. F. A., Choat, B., and Jansen, S.: Meta-
653 analysis reveals that hydraulic traits explain cross-species patterns of drought-induced tree mortality across the
654 globe, *PNAS*, 113, 5024–5029, <https://doi.org/10.1073/pnas.1525678113>, 2016.
- 655 Armstrong McKay, D. I., Staal, A., Abrams, J. F., Winkelmann, R., Sakschewski, B., Loriani, S., Fetzer, I.,
656 Cornell, S. E., Rockström, J., and Lenton, T. M.: Exceeding 1.5°C global warming could trigger multiple
657 climate tipping points, *Science*, 377, eabn7950, <https://doi.org/10.1126/science.abn7950>, 2022.
- 658 Arora, V. K., Seiler, C., Wang, L., and Kou-Giesbrecht, S.: Towards an ensemble-based evaluation of land
659 surface models in light of uncertain forcings and observations, *Biogeosciences*, 20, 1313–1355,
660 <https://doi.org/10.5194/bg-20-1313-2023>, 2023.
- 661 Baker, J. C. A., Garcia-Carreras, L., Buermann, W., Souza, D. C. de, Marsham, J. H., Kubota, P. Y., Gloor, M.,
662 Coelho, C. A. S., and Spracklen, D. V.: Robust Amazon precipitation projections in climate models that capture
663 realistic land–atmosphere interactions, *Environ. Res. Lett.*, 16, 074002, [https://doi.org/10.1088/1748-](https://doi.org/10.1088/1748-9326/abfb2e)
664 9326/abfb2e, 2021.
- 665 Barros, F. de V., Bittencourt, P. R. L., Brum, M., Restrepo-Coupe, N., Pereira, L., Teodoro, G. S., Saleska, S.
666 R., Borma, L. S., Christoffersen, B. O., Penha, D., Alves, L. F., Lima, A. J. N., Carneiro, V. M. C., Gentine, P.,
667 Lee, J.-E., Aragão, L. E. O. C., Ivanov, V., Leal, L. S. M., Araujo, A. C., and Oliveira, R. S.: Hydraulic traits
668 explain differential responses of Amazonian forests to the 2015 El Niño-induced drought, *New Phytologist*,
669 223, 1253–1266, <https://doi.org/10.1111/nph.15909>, 2019.
- 670 Bauman, D., Fortunel, C., Delhaye, G., Malhi, Y., Cernusak, L. A., Bentley, L. P., Rifai, S. W., Aguirre-
671 Gutiérrez, J., Menor, I. O., Phillips, O. L., McNellis, B. E., Bradford, M., Laurance, S. G. W., Hutchinson, M.
672 F., Dempsey, R., Santos-Andrade, P. E., Ninantay-Rivera, H. R., Chambi Paucar, J. R., and McMahon, S. M.:
673 Tropical tree mortality has increased with rising atmospheric water stress, *Nature*, 1–6,
674 <https://doi.org/10.1038/s41586-022-04737-7>, 2022.
- 675 de Boer-Euser, T., McMillan, H. K., Hrachowitz, M., Winsemius, H. C., and Savenije, H. H. G.: Influence of
676 soil and climate on root zone storage capacity, *Water Resources Research*, 52, 2009–2024,
677 <https://doi.org/10.1002/2015WR018115>, 2016.
- 678 Bouaziz, L. J. E., Steele-Dunne, S. C., Schellekens, J., Weerts, A. H., Stam, J., Sprokkereef, E., Winsemius, H.
679 H. C., Savenije, H. H. G., and Hrachowitz, M.: Improved Understanding of the Link Between Catchment-Scale
680 Vegetation Accessible Storage and Satellite-Derived Soil Water Index, *Water Resources Research*, 56,
681 e2019WR026365, <https://doi.org/10.1029/2019WR026365>, 2020.

- 682 Boulton, C. A., Good, P., and Lenton, T. M.: Early warning signals of simulated Amazon rainforest dieback,
683 *Theor Ecol*, 6, 373–384, <https://doi.org/10.1007/s12080-013-0191-7>, 2013.
- 684 Boulton, C. A., Booth, B. B. B., and Good, P.: Exploring uncertainty of Amazon dieback in a perturbed
685 parameter Earth system ensemble, *Global Change Biology*, 23, 5032–5044, <https://doi.org/10.1111/gcb.13733>,
686 2017.
- 687 Boulton, C. A., Lenton, T. M., and Boers, N.: Pronounced loss of Amazon rainforest resilience since the early
688 2000s, *Nat. Clim. Chang.*, 12, 271–278, <https://doi.org/10.1038/s41558-022-01287-8>, 2022.
- 689 Bovolo, C. I., Wagner, T., Parkin, G., Hein-Griggs, D., Pereira, R., and Jones, R.: The Guiana Shield
690 rainforests—overlooked guardians of South American climate, *Environ. Res. Lett.*, 13, 074029,
691 <https://doi.org/10.1088/1748-9326/aac60>, 2018.
- 692 Brienen, R. J. W., Phillips, O. L., Feldpausch, T. R., Gloor, E., Baker, T. R., Lloyd, J., Lopez-Gonzalez, G.,
693 Monteagudo-Mendoza, A., Malhi, Y., Lewis, S. L., Vásquez Martínez, R., Alexiades, M., Álvarez Dávila, E.,
694 Alvarez-Loayza, P., Andrade, A., Aragão, L. E. O. C., Araujo-Murakami, A., Arets, E. J. M. M., Arroyo, L.,
695 Aymard C., G. A., Bánki, O. S., Baraloto, C., Barroso, J., Bonal, D., Boot, R. G. A., Camargo, J. L. C.,
696 Castilho, C. V., Chama, V., Chao, K. J., Chave, J., Comiskey, J. A., Cornejo Valverde, F., da Costa, L., de
697 Oliveira, E. A., Di Fiore, A., Erwin, T. L., Fauset, S., Forsthofer, M., Galbraith, D. R., Grahame, E. S., Groot,
698 N., Hérault, B., Higuchi, N., Honorio Coronado, E. N., Keeling, H., Killeen, T. J., Laurance, W. F., Laurance,
699 S., Licona, J., Magnussen, W. E., Marimon, B. S., Marimon-Junior, B. H., Mendoza, C., Neill, D. A., Nogueira,
700 E. M., Núñez, P., Pallqui Camacho, N. C., Parada, A., Pardo-Molina, G., Peacock, J., Peña-Claros, M.,
701 Pickavance, G. C., Pitman, N. C. A., Poorter, L., Prieto, A., Quesada, C. A., Ramírez, F., Ramírez-Angulo, H.,
702 Restrepo, Z., Roopsind, A., Rudas, A., Salomão, R. P., Schwarz, M., Silva, N., Silva-Espejo, J. E., Silveira, M.,
703 Stropp, J., Talbot, J., ter Steege, H., Teran-Aguilar, J., Terborgh, J., Thomas-Caesar, R., Toledo, M., Torello-
704 Raventos, M., Umetsu, R. K., van der Heijden, G. M. F., van der Hout, P., Guimarães Vieira, I. C., Vieira, S.
705 A., Vilanova, E., Vos, V. A., and Zagt, R. J.: Long-term decline of the Amazon carbon sink, *Nature*, 519, 344–
706 348, <https://doi.org/10.1038/nature14283>, 2015.
- 707 Bronick, C. J. and Lal, R.: Soil structure and management: a review, *Geoderma*, 124, 3–22,
708 <https://doi.org/10.1016/j.geoderma.2004.03.005>, 2005.
- 709 Brooks, P. D., Chorover, J., Fan, Y., Godsey, S. E., Maxwell, R. M., McNamara, J. P., and Tague, C.:
710 Hydrological partitioning in the critical zone: Recent advances and opportunities for developing transferable
711 understanding of water cycle dynamics, *Water Resources Research*, 51, 6973–6987,
712 <https://doi.org/10.1002/2015WR017039>, 2015.
- 713 Brum, M., Vadeboncoeur, M. A., Ivanov, V., Asbjornsen, H., Saleska, S., Alves, L. F., Penha, D., Dias, J. D.,
714 Aragão, L. E. O. C., Barros, F., Bittencourt, P., Pereira, L., and Oliveira, R. S.: Hydrological niche segregation
715 defines forest structure and drought tolerance strategies in a seasonal Amazon forest, *Journal of Ecology*, 107,
716 318–333, <https://doi.org/10.1111/1365-2745.13022>, 2019.
- 717 Brunner, I., Herzog, C., Dawes, M. A., Arend, M., and Sperisen, C.: How tree roots respond to drought,
718 *Frontiers in Plant Science*, 6, 2015.
- 719 Bruno, R. D., Rocha, H. R. da, Freitas, H. C. de, Goulden, M. L., and Miller, S. D.: Soil moisture dynamics in
720 an eastern Amazonian tropical forest, *Hydrological Processes*, 20, 2477–2489,
721 <https://doi.org/10.1002/hyp.6211>, 2006.
- 722 Canadell, J., Jackson, R. B., Ehleringer, J. B., Mooney, H. A., Sala, O. E., and Schulze, E.-D.: Maximum
723 rooting depth of vegetation types at the global scale, *Oecologia*, 108, 583–595,
724 <https://doi.org/10.1007/BF00329030>, 1996.

725 Canadell, J. G., Monteiro, P. M. S., Costa, M. H., Cunha, L. C. D., Cox, P. M., Eliseev, A. V., Henson, S., Ishii,
726 M., Jaccard, S., Koven, C., Lohila, A., Patra, P. K., Piao, S., Syampungani, S., Zaehle, S., Zickfeld, K.,
727 Alexandrov, G. A., Bala, G., Bopp, L., Boysen, L., Cao, L., Chandra, N., Ciais, P., Denisov, S. N., Dentener, F.
728 J., Douville, H., Fay, A., Forster, P., Fox-Kemper, B., Friedlingstein, P., Fu, W., Fuss, S., Garçon, V., Gier, B.,
729 Gillett, N. P., Gregor, L., Haustein, K., Haverd, V., He, J., Hewitt, H. T., Hoffman, F. M., Ilyina, T., Jackson,
730 R., Jones, C., Keller, D. P., Kwiatkowski, L., Lamboll, R. D., Lan, X., Laufkötter, C., Quéré, C. L., Lenton, A.,
731 Lewis, J., Liddicoat, S., Lorenzoni, L., Lovenduski, N., Macdougall, A. H., Mathesius, S., Matthews, D. H.,
732 Meinshausen, M., Mokhov, I. I., Naik, V., Nicholls, Z. R. J., Nurhati, I. S., O'sullivan, M., Peters, G., Pongratz,
733 J., Poulter, B., Sallée, J.-B., Saunoy, M., Schuur, E. A. G., Seneviratne, S., Stavert, A., Suntharalingam, P.,
734 Tachiiri, K., Terhaar, J., Thompson, R., Tian, H., Turnbull, J., Vicente-Serrano, S. M., Wang, X., Wanninkhof,
735 R. H., Williamson, P., Brovkin, V., Feely, R. A., and Lebehof, A. D.: Global Carbon and other Biogeochemical
736 Cycles and Feedbacks, in: IPCC AR6 WGI, Final Government Distribution, chapter 5, 2021.

737 Chai, Y., Martins, G., Nobre, C., von Randow, C., Chen, T., and Dolman, H.: Constraining Amazonian land
738 surface temperature sensitivity to precipitation and the probability of forest dieback, *npj Clim Atmos Sci*, 4, 1–
739 7, <https://doi.org/10.1038/s41612-021-00162-1>, 2021.

740 Cheng, S., Huang, J., Ji, F., and Lin, L.: Uncertainties of soil moisture in historical simulations and future
741 projections, *Journal of Geophysical Research: Atmospheres*, 122, 2239–2253,
742 <https://doi.org/10.1002/2016JD025871>, 2017.

743 Cole, L. E. S., Bhagwat, S. A., and Willis, K. J.: Recovery and resilience of tropical forests after disturbance,
744 *Nature Communications*, 5, 3906, <https://doi.org/10.1038/ncomms4906>, 2014.

745 Condit, R., Engelbrecht, B. M. J., Pino, D., Pérez, R., and Turner, B. L.: Species distributions in response to
746 individual soil nutrients and seasonal drought across a community of tropical trees, *PNAS*, 110, 5064–5068,
747 <https://doi.org/10.1073/pnas.1218042110>, 2013.

748 Cook, K. H. and Vizy, E. K.: Impact of climate change on mid-twenty-first century growing seasons in Africa,
749 *Clim Dyn*, 39, 2937–2955, <https://doi.org/10.1007/s00382-012-1324-1>, 2012.

750 Cooper, G. S., Willcock, S., and Dearing, J. A.: Regime shifts occur disproportionately faster in larger
751 ecosystems, *Nature Communications*, 11, 1175, <https://doi.org/10.1038/s41467-020-15029-x>, 2020.

752 skextremes Documentation: <https://github.com/kikocorreoso/scikit-extremes>.

753 Cox, P. M., Betts, R. A., Collins, M., Harris, P. P., Huntingford, C., and Jones, C. D.: Amazonian forest
754 dieback under climate-carbon cycle projections for the 21st century, *Theor Appl Climatol*, 78, 137–156,
755 <https://doi.org/10.1007/s00704-004-0049-4>, 2004.

756 Dai, A.: Drought under global warming: a review, *WIREs Climate Change*, 2, 45–65,
757 <https://doi.org/10.1002/wcc.81>, 2011.

758 Davidson, E. A., de Araújo, A. C., Artaxo, P., Balch, J. K., Brown, I. F., C. Bustamante, M. M., Coe, M. T.,
759 DeFries, R. S., Keller, M., Longo, M., Munger, J. W., Schroeder, W., Soares-Filho, B. S., Souza, C. M., and
760 Wofsy, S. C.: The Amazon basin in transition, *Nature*, 481, 321–328, <https://doi.org/10.1038/nature10717>,
761 2012.

762 Dexter, A. R.: Soil physical quality: Part II. Friability, tillage, tith and hard-setting, *Geoderma*, 120, 215–225,
763 <https://doi.org/10.1016/j.geoderma.2003.09.005>, 2004.

764 Dittert, K., Wätzel, J., and Sattelmacher, B.: Responses of *Alnus glutinosa* to Anaerobic Conditions -
765 Mechanisms and Rate of Oxygen Flux into the Roots, *Plant Biology*, 8, 212–223, [https://doi.org/10.1055/s-](https://doi.org/10.1055/s-2005-873041)
766 2005-873041, 2006.

- 767 Doughty, C. E., Keany, J. M., Wiebe, B. C., Rey-Sanchez, C., Carter, K. R., Middleby, K. B., Cheesman, A.
768 W., Goulden, M. L., da Rocha, H. R., Miller, S. D., Malhi, Y., Fauset, S., Gloor, E., Slot, M., Oliveras Menor,
769 I., Crous, K. Y., Goldsmith, G. R., and Fisher, J. B.: Tropical forests are approaching critical temperature
770 thresholds, *Nature*, 621, 105–111, <https://doi.org/10.1038/s41586-023-06391-z>, 2023.
- 771 Driyfhout, S., Bathiany, S., Beaulieu, C., Brovkin, V., Claussen, M., Huntingford, C., Scheffer, M., Sgubin, G.,
772 and Swingedouw, D.: Catalogue of abrupt shifts in Intergovernmental Panel on Climate Change climate
773 models, *Proceedings of the National Academy of Sciences*, 112, E5777–E5786,
774 <https://doi.org/10.1073/pnas.1511451112>, 2015.
- 775 Dunning, C. M., Black, E., and Allan, R. P.: Later Wet Seasons with More Intense Rainfall over Africa under
776 Future Climate Change, *Journal of Climate*, 31, 9719–9738, 2018.
- 777 van der Ent, R. J., Savenije, H. H. G., Schaeffli, B., and Steele-Dunne, S. C.: Origin and fate of atmospheric
778 moisture over continents, *Water Resources Research*, 46, <https://doi.org/10.1029/2010WR009127>, 2010.
- 779 GlobCover land-use map: http://due.esrin.esa.int/page_globcover.php, last access: 27 February 2022.
- 780 Esquivel-Muelbert, A., Baker, T. R., Dexter, K. G., Lewis, S. L., Brienen, R. J. W., Feldpausch, T. R., Lloyd,
781 J., Monteagudo-Mendoza, A., Arroyo, L., Álvarez-Dávila, E., Higuchi, N., Marimon, B. S., Marimon-Junior,
782 B. H., Silveira, M., Vilanova, E., Gloor, E., Malhi, Y., Chave, J., Barlow, J., Bonal, D., Cardozo, N. D., Erwin,
783 T., Fauset, S., Hérault, B., Laurance, S., Poorter, L., Qie, L., Stahl, C., Sullivan, M. J. P., Steege, H. ter, Vos, V.
784 A., Zuidema, P. A., Almeida, E., Oliveira, E. A. de, Andrade, A., Vieira, S. A., Aragão, L., Araujo-Murakami,
785 A., Arets, E., C. G. A. A., Baraloto, C., Camargo, P. B., Barroso, J. G., Bongers, F., Boot, R., Camargo, J. L.,
786 Castro, W., Moscoso, V. C., Comiskey, J., Valverde, F. C., Costa, A. C. L. da, Pasquel, J. del A., Fiore, A. D.,
787 Duque, L. F., Elias, F., Engel, J., Llampazo, G. F., Galbraith, D., Fernández, R. H., Coronado, E. H., Hubau,
788 W., Jimenez-Rojas, E., Lima, A. J. N., Umetsu, R. K., Laurance, W., Lopez-Gonzalez, G., Lovejoy, T., Cruz,
789 O. A. M., Morandi, P. S., Neill, D., Vargas, P. N., Camacho, N. C. P., Gutierrez, A. P., Pardo, G., Peacock, J.,
790 Peña-Claros, M., Peñuela-Mora, M. C., Petronelli, P., Pickavance, G. C., Pitman, N., Prieto, A., Quesada, C.,
791 Ramírez-Angulo, H., Réjou-Méchain, M., Correa, Z. R., Roopsind, A., Rudas, A., Salomão, R., Silva, N.,
792 Espejo, J. S., Singh, J., Stropp, J., Terborgh, J., Thomas, R., Toledo, M., Torres-Lezama, A., Gamarra, L. V.,
793 Meer, P. J. van de, Heijden, G. van der, et al.: Compositional response of Amazon forests to climate change,
794 *Global Change Biology*, 25, 39–56, <https://doi.org/10.1111/gcb.14413>, 2019.
- 795 Fan, Y., Miguez-Macho, G., Jobbágy, E. G., Jackson, R. B., and Otero-Casal, C.: Hydrologic regulation of
796 plant rooting depth, *Proceedings of the National Academy of Sciences*, 114, 10572–10577,
797 <https://doi.org/10.1073/pnas.1712381114>, 2017.
- 798 Fayos, C. B.: The roles of texture and structure in the water retention capacity of burnt Mediterranean soils with
799 varying rainfall, *CATENA*, 31, 219–236, [https://doi.org/10.1016/S0341-8162\(97\)00041-6](https://doi.org/10.1016/S0341-8162(97)00041-6), 1997.
- 800 February, E. C. and Higgins, S. I.: The distribution of tree and grass roots in savannas in relation to soil
801 nitrogen and water, *South African Journal of Botany*, 76, 517–523, <https://doi.org/10.1016/j.sajb.2010.04.001>,
802 2010.
- 803 Ferreira, D., Marshall, J., and Rose, B.: Climate Determinism Revisited: Multiple Equilibria in a Complex
804 Climate Model, *Journal of Climate*, 24, 992–1012, <https://doi.org/10.1175/2010JCLI3580.1>, 2011.
- 805 Fleischer, K., Rammig, A., De Kauwe, M. G., Walker, A. P., Domingues, T. F., Fuchslueger, L., Garcia, S.,
806 Goll, D. S., Grandis, A., Jiang, M., Haverd, V., Hofhansl, F., Holm, J. A., Kruijt, B., Leung, F., Medlyn, B. E.,
807 Mercado, L. M., Norby, R. J., Pak, B., von Randow, C., Quesada, C. A., Schaap, K. J., Valverde-Barrantes, O.
808 J., Wang, Y.-P., Yang, X., Zaehle, S., Zhu, Q., and Lapola, D. M.: Amazon forest response to CO₂ fertilization
809 dependent on plant phosphorus acquisition, *Nat. Geosci.*, 12, 736–741, <https://doi.org/10.1038/s41561-019-0404-9>,
810 2019.

- 811 Flores, B. M., Montoya, E., Sakschewski, B., Nascimento, N., Staal, A., Betts, R. A., Levis, C., Lapola, D. M.,
812 Esquivel-Muelbert, A., Jakovac, C., Nobre, C. A., Oliveira, R. S., Borma, L. S., Nian, D., Boers, N., Hecht, S.
813 B., ter Steege, H., Arriera, J., Lucas, I. L., Berenguer, E., Marengo, J. A., Gatti, L. V., Mattos, C. R. C., and
814 Hirota, M.: Critical transitions in the Amazon forest system, *Nature*, 626, 555–564,
815 <https://doi.org/10.1038/s41586-023-06970-0>, 2024.
- 816 Funk, C., Peterson, P., Landsfeld, M., Pedreros, D., Verdin, J., Shukla, S., Husak, G., Rowland, J., Harrison, L.,
817 Hoell, A., and Michaelsen, J.: The climate hazards infrared precipitation with stations—a new environmental
818 record for monitoring extremes, *Scientific Data*, 2, 150066, <https://doi.org/10.1038/sdata.2015.66>, 2015.
- 819 Gao, H., Hrachowitz, M., Schymanski, S. J., Fenicia, F., Sriwongsitanon, N., and Savenije, H. H. G.: Climate
820 controls how ecosystems size the root zone storage capacity at catchment scale: Root zone storage capacity in
821 catchments, *Geophysical Research Letters*, 41, 7916–7923, <https://doi.org/10.1002/2014GL061668>, 2014.
- 822 Grimm, N. B., Chapin III, F. S., Bierwagen, B., Gonzalez, P., Groffman, P. M., Luo, Y., Melton, F.,
823 Nadelhoffer, K., Pairis, A., Raymond, P. A., Schimel, J., and Williamson, C. E.: The impacts of climate change
824 on ecosystem structure and function, *Frontiers in Ecology and the Environment*, 11, 474–482,
825 <https://doi.org/10.1890/120282>, 2013.
- 826 Gumbel, E. J.: *Statistics of extremes.*, Columbia University Press, New York, 1958.
- 827 Guswa, A. J.: The influence of climate on root depth: A carbon cost-benefit analysis, *Water Resources*
828 *Research*, 44, W02427, <https://doi.org/10.1029/2007WR006384>, 2008.
- 829 Hahm, W. J., Rempe, D. M., Dralle, D. N., Dawson, T. E., Lovill, S. M., Bryk, A. B., Bish, D. L., Schieber, J.,
830 and Dietrich, W. E.: Lithologically Controlled Subsurface Critical Zone Thickness and Water Storage Capacity
831 Determine Regional Plant Community Composition, *Water Resources Research*, 55, 3028–3055,
832 <https://doi.org/10.1029/2018WR023760>, 2019.
- 833 Hall, A., Cox, P., Huntingford, C., and Klein, S.: Progressing emergent constraints on future climate change,
834 *Nat. Clim. Chang.*, 9, 269–278, <https://doi.org/10.1038/s41558-019-0436-6>, 2019.
- 835 Hersbach, H., Bell, B., Berrisford, P., Hirahara, S., Horányi, A., Muñoz-Sabater, J., Nicolas, J., Peubey, C.,
836 Radu, R., Schepers, D., Simmons, A., Soci, C., Abdalla, S., Abellan, X., Balsamo, G., Bechtold, P., Biavati, G.,
837 Bidlot, J., Bonavita, M., Chiara, G. D., Dahlgren, P., Dee, D., Diamantakis, M., Dragani, R., Flemming, J.,
838 Forbes, R., Fuentes, M., Geer, A., Haimberger, L., Healy, S., Hogan, R. J., Hólm, E., Janisková, M., Keeley, S.,
839 Laloyaux, P., Lopez, P., Lupu, C., Radnoti, G., Rosnay, P. de, Rozum, I., Vamborg, F., Villaume, S., and
840 Thépaut, J.-N.: The ERA5 Global Reanalysis, *Quarterly Journal of the Royal Meteorological Society*, 245,
841 111840, <https://doi.org/10.1002/qj.3803>, 2020.
- 842 Higgins, S. I. and Scheiter, S.: Atmospheric CO₂ forces abrupt vegetation shifts locally, but not globally,
843 *Nature*, 488, 209–212, <https://doi.org/10.1038/nature11238>, 2012.
- 844 Hildebrandt, A., Kleidon, A., and Bechmann, M.: A thermodynamic formulation of root water uptake,
845 *Hydrology and Earth System Sciences*, 20, 3441–3454, <https://doi.org/10.5194/hess-20-3441-2016>, 2016.
- 846 Hirota, M., Holmgren, M., Van Nes, E. H., and Scheffer, M.: Global Resilience of Tropical Forest and Savanna
847 to Critical Transitions, *Science*, 334, 232–235, <https://doi.org/10.1126/science.1210657>, 2011.
- 848 Hirota, M., Flores, B. M., Betts, R., Borma, L. S., Esquivel-Muelbert, A., Jakovac, C., Lapola, D. M., Montoya,
849 E., Oliveira, R. S., and Sakschewski, B.: Chapter 24: Resilience of the Amazon forest to global changes:
850 Assessing the risk of tipping points, in: *Amazon Assessment Report 2021*, edited by: Nobre, C., Encalada, A.,
851 Anderson, E., Roca Alcazar, F. H., Bustamante, M., Mena, C., Peña-Claros, M., Poveda, G., Rodriguez, J. P.,
852 Saleska, S., Trumbore, S. E., Val, A., Villa Nova, L., Abramovay, R., Alencar, A., Rodriguez Alzza, A. C.,
853 Armenteras, D., Artaxo, P., Athayde, S., Barretto Filho, H. T., Barlow, J., Berenguer, E., Bortolotto, F., Costa,

854 F. de A., Costa, M. H., Cuvi, N., Fearnside, P., Ferreira, J., Flores, B. M., Frieri, S., Gatti, L. V., Guayasamin,
855 J. M., Hecht, S., Hirota, M., Hoorn, C., Josse, C., Lapola, D. M., Larrea, C., Larrea-Alcazar, D. M., Lehm
856 Ardaya, Z., Malhi, Y., Marengo, J. A., Melack, J., Moraes R., M., Moutinho, P., Murmis, M. R., Neves, E. G.,
857 Paez, B., Painter, L., Ramos, A., Rosero-Peña, M. C., Schmink, M., Sist, P., ter Steege, H., Val, P., van der
858 Voort, H., Varese, M., and Zapata-Ríos, G., UN Sustainable Development Solutions Network (SDSN),
859 <https://doi.org/10.55161/QPYS9758>, 2021.

860 Hofhansl, F., Andersen, K. M., Fleischer, K., Fuchslueger, L., Rammig, A., Schaap, K. J., Valverde-Barrantes,
861 O. J., and Lapola, D. M.: Amazon Forest Ecosystem Responses to Elevated Atmospheric CO₂ and Alterations
862 in Nutrient Availability: Filling the Gaps with Model-Experiment Integration, *Frontiers in Earth Science*, 4,
863 2016.

864 Hubau, W., Lewis, S. L., Phillips, O. L., Affum-Baffoe, K., Beeckman, H., Cuní-Sánchez, A., Daniels, A. K.,
865 Ewango, C. E. N., Fauset, S., Mukinzi, J. M., Sheil, D., Sonké, B., Sullivan, M. J. P., Sunderland, T. C. H.,
866 Taedoumg, H., Thomas, S. C., White, L. J. T., Abernethy, K. A., Adu-Bredu, S., Amani, C. A., Baker, T. R.,
867 Banin, L. F., Baya, F., Begne, S. K., Bennett, A. C., Benedet, F., Bitariho, R., Bocko, Y. E., Boeckx, P.,
868 Boundja, P., Brienen, R. J. W., Brncic, T., Chezeaux, E., Chuyong, G. B., Clark, C. J., Collins, M., Comiskey,
869 J. A., Coomes, D. A., Dargie, G. C., de Haulleville, T., Kamdem, M. N. D., Doucet, J.-L., Esquivel-Muelbert,
870 A., Feldpausch, T. R., Fofanah, A., Foli, E. G., Gilpin, M., Gloor, E., Gonmadje, C., Gourlet-Fleury, S., Hall, J.
871 S., Hamilton, A. C., Harris, D. J., Hart, T. B., Hockemba, M. B. N., Hladik, A., Ifo, S. A., Jeffery, K. J., Jucker,
872 T., Yakusu, E. K., Kearsley, E., Kenfack, D., Koch, A., Leal, M. E., Levesley, A., Lindsell, J. A., Lisingo, J.,
873 Lopez-Gonzalez, G., Lovett, J. C., Makana, J.-R., Malhi, Y., Marshall, A. R., Martin, J., Martin, E. H., Mbayu,
874 F. M., Medjibe, V. P., Mihindou, V., Mitchard, E. T. A., Moore, S., Munishi, P. K. T., Bengone, N. N., Ojo, L.,
875 Ondo, F. E., Peh, K. S.-H., Pickavance, G. C., Poulsen, A. D., Poulsen, J. R., Qie, L., Reitsma, J., Rovero, F.,
876 Swaine, M. D., Talbot, J., Taplin, J., Taylor, D. M., Thomas, D. W., Toirambe, B., Mukendi, J. T., Tuagben,
877 D., Umunay, P. M., et al.: Asynchronous carbon sink saturation in African and Amazonian tropical forests,
878 *Nature*, 579, 80–87, <https://doi.org/10.1038/s41586-020-2035-0>, 2020.

879 Huntingford, C., Zelazowski, P., Galbraith, D., Mercado, L. M., Sitch, S., Fisher, R., Lomas, M., Walker, A. P.,
880 Jones, C. D., Booth, B. B. B., Malhi, Y., Hemming, D., Kay, G., Good, P., Lewis, S. L., Phillips, O. L., Atkin,
881 O. K., Lloyd, J., Gloor, E., Zaragoza-Castells, J., Meir, P., Betts, R., Harris, P. P., Nobre, C., Marengo, J., and
882 Cox, P. M.: Simulated resilience of tropical rainforests to CO₂-induced climate change, *Nature Geosci*, 6, 268–
883 273, <https://doi.org/10.1038/ngeo1741>, 2013.

884 Hurtt, G. C., Chini, L., Sahajpal, R., Frohling, S., Boudris, B. L., Calvin, K., Doelman, J. C., Fisk, J.,
885 Fujimori, S., Klein Goldewijk, K., Hasegawa, T., Havlik, P., Heinemann, A., Humpenöder, F., Jungclaus, J.,
886 Kaplan, J. O., Kennedy, J., Krisztin, T., Lawrence, D., Lawrence, P., Ma, L., Mertz, O., Pongratz, J., Popp, A.,
887 Poulter, B., Riahi, K., Shevliakova, E., Stehfest, E., Thornton, P., Tubiello, F. N., van Vuuren, D. P., and
888 Zhang, X.: Harmonization of global land use change and management for the period 850–2100 (LUH2) for
889 CMIP6, *Geoscientific Model Development*, 13, 5425–5464, <https://doi.org/10.5194/gmd-13-5425-2020>, 2020.

890 Indoria, A. K., Sharma, K. L., and Reddy, K. S.: Chapter 18 - Hydraulic properties of soil under warming
891 climate, in: *Climate Change and Soil Interactions*, edited by: Prasad, M. N. V. and Pietrzykowski, M., Elsevier,
892 473–508, <https://doi.org/10.1016/B978-0-12-818032-7.00018-7>, 2020.

893 Jach, L., Warrach-Sagi, K., Ingwersen, J., Kaas, E., and Wulfmeyer, V.: Land Cover Impacts on Land-
894 Atmosphere Coupling Strength in Climate Simulations With WRF Over Europe, *Journal of Geophysical*
895 *Research: Atmospheres*, 125, e2019JD031989, <https://doi.org/10.1029/2019JD031989>, 2020.

896 Jackson, R. B., Canadell, J., Ehleringer, J. R., Mooney, H. A., Sala, O. E., and Schulze, E. D.: A global analysis
897 of root distributions for terrestrial biomes, *Oecologia*, 108, 389–411, <https://doi.org/10.1007/BF00333714>,
898 1996.

899 Jehn, F. U., Kemp, L., Ilin, E., Funk, C., Wang, J. R., and Breuer, L.: Focus of the IPCC Assessment Reports
900 Has Shifted to Lower Temperatures, *Earth's Future*, 10, e2022EF002876,
901 <https://doi.org/10.1029/2022EF002876>, 2022.

902 Jiang, C. and Ryu, Y.: Multi-scale evaluation of global gross primary productivity and evapotranspiration
903 products derived from Breathing Earth System Simulator (BESS), *Remote Sensing of Environment*, 186, 528–
904 547, <https://doi.org/10.1016/j.rse.2016.08.030>, 2016.

905 Jones, C., Lowe, J., Liddicoat, S., and Betts, R.: Committed terrestrial ecosystem changes due to climate
906 change, *Nature Geosci*, 2, 484–487, <https://doi.org/10.1038/ngeo555>, 2009.

907 Jung, M., Koirala, S., Weber, U., Ichii, K., Gans, F., Camps-Valls, G., Papale, D., Schwalm, C., Tramontana,
908 G., and Reichstein, M.: The FLUXCOM ensemble of global land-atmosphere energy fluxes, *Sci Data*, 6, 74,
909 <https://doi.org/10.1038/s41597-019-0076-8>, 2019.

910 Koch, A., Hubau, W., and Lewis, S. L.: Earth System Models Are Not Capturing Present-Day Tropical Forest
911 Carbon Dynamics, *Earth's Future*, 9, e2020EF001874, <https://doi.org/10.1029/2020EF001874>, 2021.

912 Kooperman, G. J., Chen, Y., Hoffman, F. M., Koven, C. D., Lindsay, K., Pritchard, M. S., Swann, A. L. S., and
913 Randerson, J. T.: Forest response to rising CO₂ drives zonally asymmetric rainfall change over tropical land,
914 *Nature Clim Change*, 8, 434–440, <https://doi.org/10.1038/s41558-018-0144-7>, 2018.

915 Körner, C.: A matter of tree longevity, *Science*, 355, 130–131, <https://doi.org/10.1126/science.aal2449>, 2017.

916 Küçük, Ç., Koirala, S., Carvalhais, N., Miralles, D. G., Reichstein, M., and Jung, M.: Characterizing the
917 Response of Vegetation Cover to Water Limitation in Africa Using Geostationary Satellites, *Journal of*
918 *Advances in Modeling Earth Systems*, 14, e2021MS002730, <https://doi.org/10.1029/2021MS002730>, 2022.

919 Kukal, M. S. and Irmak, S.: Can limits of plant available water be inferred from soil moisture distributions?,
920 *Agricultural & Environmental Letters*, 8, e20113, <https://doi.org/10.1002/ael2.20113>, 2023.

921 Lammertsma, E. I., Boer, H. J. de, Dekker, S. C., Dilcher, D. L., Lotter, A. F., and Wagner-Cremer, F.: Global
922 CO₂ rise leads to reduced maximum stomatal conductance in Florida vegetation, *PNAS*, 108, 4035–4040,
923 <https://doi.org/10.1073/pnas.1100371108>, 2011.

924 Leite-Filho, A. T., Soares-Filho, B. S., Davis, J. L., Abrahão, G. M., and Börner, J.: Deforestation reduces
925 rainfall and agricultural revenues in the Brazilian Amazon, *Nat Commun*, 12, 2591,
926 <https://doi.org/10.1038/s41467-021-22840-7>, 2021.

927 Lenton, T. M.: Early warning of climate tipping points, *Nature Clim Change*, 1, 201–209,
928 <https://doi.org/10.1038/nclimate1143>, 2011.

929 Lenton, T. M., Rockström, J., Gaffney, O., Rahmstorf, S., Richardson, K., Steffen, W., and Schellnhuber, H. J.:
930 Climate tipping points — too risky to bet against, *Nature*, 575, 592–595, <https://doi.org/10.1038/d41586-019-03595-0>, 2019.

932 Lewis, S. L., Edwards, D. P., and Galbraith, D.: Increasing human dominance of tropical forests, *Science*, 349,
933 827–832, <https://doi.org/10.1126/science.aaa9932>, 2015.

934 Li, Y., Brando, P. M., Morton, D. C., Lawrence, D. M., Yang, H., and Randerson, J. T.: Deforestation-induced
935 climate change reduces carbon storage in remaining tropical forests, *Nat Commun*, 13, 1964,
936 <https://doi.org/10.1038/s41467-022-29601-0>, 2022.

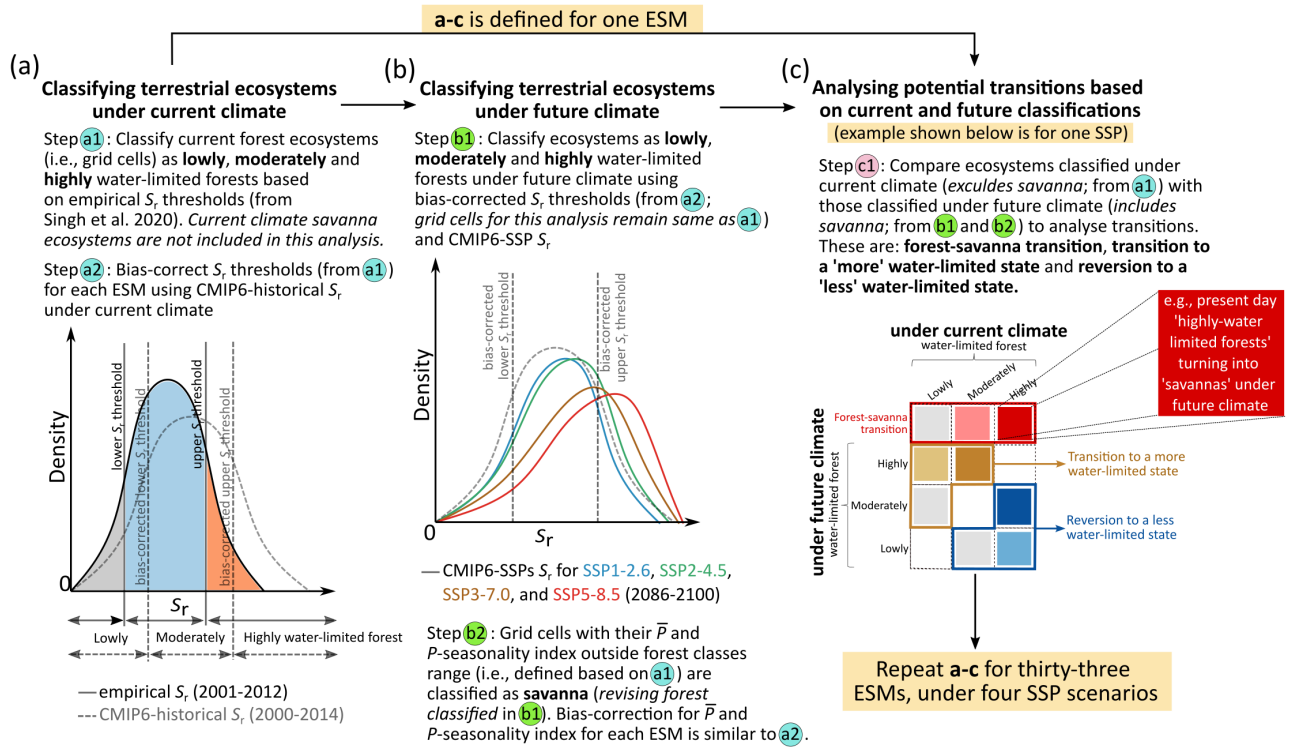
- 937 Liu, W., Sun, F., Lim, W. H., Zhang, J., Wang, H., Shiogama, H., and Zhang, Y.: Global drought and severe
938 drought-affected populations in 1.5 and 2 °C warmer worlds, *Earth System Dynamics*, 9, 267–283,
939 <https://doi.org/10.5194/esd-9-267-2018>, 2018.
- 940 Liu, Y., Kumar, M., Katul, G. G., Feng, X., and Konings, A. G.: Plant hydraulics accentuates the effect of
941 atmospheric moisture stress on transpiration, *Nat. Clim. Chang.*, 10, 691–695, <https://doi.org/10.1038/s41558-020-0781-5>, 2020.
- 943 Ma, L., Hurtt, G. C., Chini, L. P., Sahajpal, R., Pongratz, J., Frohking, S., Stehfest, E., Klein Goldewijk, K.,
944 O’Leary, D., and Doelman, J. C.: Global rules for translating land-use change (LUH2) to land-cover change for
945 CMIP6 using GLM2, *Geoscientific Model Development*, 13, 3203–3220, <https://doi.org/10.5194/gmd-13-3203-2020>, 2020.
- 947 Malhi, Y., Roberts, J. T., Betts, R. A., Killeen, T. J., Li, W., and Nobre, C. A.: Climate Change, Deforestation,
948 and the Fate of the Amazon, *Science*, 319, 169–172, <https://doi.org/10.1126/science.1146961>, 2008.
- 949 Malhi, Y., Gardner, T. A., Goldsmith, G. R., Silman, M. R., and Zelazowski, P.: Tropical Forests in the
950 Anthropocene, *Annu. Rev. Environ. Resour.*, 39, 125–159, <https://doi.org/10.1146/annurev-environ-030713-155141>, 2014.
- 952 Mamalakis, A., Randerson, J. T., Yu, J.-Y., Pritchard, M. S., Magnusdottir, G., Smyth, P., Levine, P. A., Yu,
953 S., and Foufoula-Georgiou, E.: Zonally contrasting shifts of the tropical rain belt in response to climate change,
954 *Nature Climate Change*, 11, 143–151, <https://doi.org/10.1038/s41558-020-00963-x>, 2021.
- 955 Maslin, M. and Austin, P.: Climate models at their limit?, *Nature*, 486, 183–184,
956 <https://doi.org/10.1038/486183a>, 2012.
- 957 McCormick, E. L., Dralle, D. N., Hahm, W. J., Tune, A. K., Schmidt, L. M., Chadwick, K. D., and Rempe, D.
958 M.: Widespread woody plant use of water stored in bedrock, *Nature*, 597, 225–229,
959 <https://doi.org/10.1038/s41586-021-03761-3>, 2021.
- 960 McFarlane, N.: Parameterizations: representing key processes in climate models without resolving them,
961 *WIREs Climate Change*, 2, 482–497, <https://doi.org/10.1002/wcc.122>, 2011.
- 962 Nepstad, D. C., Verssimo, A., Alencar, A., Nobre, C., Lima, E., Lefebvre, P., Schlesinger, P., Potter, C.,
963 Moutinho, P., Mendoza, E., Cochrane, M., and Brooks, V.: Large-scale impoverishment of Amazonian forests
964 by logging and fire, *Nature*, 398, 505–508, <https://doi.org/10.1038/19066>, 1999.
- 965 van Nes, E. H., Arani, B. M. S., Staal, A., van der Bolt, B., Flores, B. M., Bathiany, S., and Scheffer, M.: What
966 Do You Mean, ‘Tipping Point’?, *Trends in Ecology & Evolution*, 31, 902–904,
967 <https://doi.org/10.1016/j.tree.2016.09.011>, 2016.
- 968 Nijzink, R., Hutton, C., Pechlivanidis, I., Capell, R., Arheimer, B., Freer, J., Han, D., Wagener, T., McGuire,
969 K., Savenije, H., and Hrachowitz, M.: The evolution of root-zone moisture capacities after deforestation: a step
970 towards hydrological predictions under change?, *Hydrology and Earth System Sciences*, 20, 4775–4799,
971 <https://doi.org/10.5194/hess-20-4775-2016>, 2016.
- 972 Nippert, J. B. and Holdo, R. M.: Challenging the maximum rooting depth paradigm in grasslands and savannas,
973 *Functional Ecology*, 29, 739–745, <https://doi.org/10.1111/1365-2435.12390>, 2015.
- 974 Nof, D.: Simple Versus Complex Climate Modeling, *Eos, Transactions American Geophysical Union*, 89, 544–
975 545, <https://doi.org/10.1029/2008EO520006>, 2008.
- 976 Oliveira, R. S., Dawson, T. E., Burgess, S. S. O., and Nepstad, D. C.: Hydraulic redistribution in three
977 Amazonian trees, *Oecologia*, 145, 354–363, <https://doi.org/10.1007/s00442-005-0108-2>, 2005.

- 978 Oliveras, I. and Malhi, Y.: Many shades of green: the dynamic tropical forest–savannah transition zones,
 979 Philosophical Transactions of the Royal Society B: Biological Sciences, 371, 20150308,
 980 <https://doi.org/10.1098/rstb.2015.0308>, 2016.
- 981 Parry, I. M., Ritchie, P. D. L., and Cox, P. M.: Evidence of localised Amazon rainforest dieback in CMIP6
 982 models, *Earth System Dynamics*, 13, 1667–1675, <https://doi.org/10.5194/esd-13-1667-2022>, 2022.
- 983 Pascale, S., Carvalho, L. M. V., Adams, D. K., Castro, C. L., and Cavalcanti, I. F. A.: Current and Future
 984 Variations of the Monsoons of the Americas in a Warming Climate, *Curr Clim Change Rep*, 5, 125–144,
 985 <https://doi.org/10.1007/s40641-019-00135-w>, 2019.
- 986 Piani, C., Weedon, G. P., Best, M., Gomes, S. M., Viterbo, P., Hagemann, S., and Haerter, J. O.: Statistical bias
 987 correction of global simulated daily precipitation and temperature for the application of hydrological models,
 988 *Journal of Hydrology*, 395, 199–215, <https://doi.org/10.1016/j.jhydrol.2010.10.024>, 2010.
- 989 Poorter, L., Bongers, F., Aide, T. M., Almeyda Zambrano, A. M., Balvanera, P., Becknell, J. M., Boukili, V.,
 990 Brancalion, P. H. S., Broadbent, E. N., Chazdon, R. L., Craven, D., de Almeida-Cortez, J. S., Cabral, G. A. L.,
 991 de Jong, B. H. J., Denslow, J. S., Dent, D. H., DeWalt, S. J., Dupuy, J. M., Durán, S. M., Espírito-Santo, M. M.,
 992 Fandino, M. C., César, R. G., Hall, J. S., Hernandez-Stefanoni, J. L., Jakovac, C. C., Junqueira, A. B., Kennard,
 993 D., Letcher, S. G., Licona, J.-C., Lohbeck, M., Marín-Spiotta, E., Martínez-Ramos, M., Massoca, P., Meave, J.
 994 A., Mesquita, R., Mora, F., Muñoz, R., Muscarella, R., Nunes, Y. R. F., Ochoa-Gaona, S., de Oliveira, A. A.,
 995 Orihuela-Belmonte, E., Peña-Claros, M., Pérez-García, E. A., Piotta, D., Powers, J. S., Rodríguez-Velázquez,
 996 J., Romero-Pérez, I. E., Ruíz, J., Saldarriaga, J. G., Sanchez-Azofeifa, A., Schwartz, N. B., Steininger, M. K.,
 997 Swenson, N. G., Toledo, M., Uriarte, M., van Breugel, M., van der Wal, H., Veloso, M. D. M., Vester, H. F.
 998 M., Vicentini, A., Vieira, I. C. G., Bentos, T. V., Williamson, G. B., and Rozendaal, D. M. A.: Biomass
 999 resilience of Neotropical secondary forests, *Nature*, 530, 211–214, <https://doi.org/10.1038/nature16512>, 2016.
- 1000 Rammig, A.: Tropical carbon sinks are saturating at different times on different continents, *Nature*, 579, 38–39,
 1001 <https://doi.org/10.1038/d41586-020-00423-8>, 2020.
- 1002 Ratnam, J., Bond, W. J., Fensham, R. J., Hoffmann, W. A., Archibald, S., Lehmann, C. E. R., Anderson, M. T.,
 1003 Higgins, S. I., and Sankaran, M.: When is a ‘forest’ a savanna, and why does it matter?, *Global Ecology and*
 1004 *Biogeography*, 20, 653–660, <https://doi.org/10.1111/j.1466-8238.2010.00634.x>, 2011.
- 1005 Reyer, C. P. O., Brouwers, N., Rammig, A., Brook, B. W., Epila, J., Grant, R. F., Holmgren, M., Langerwisch,
 1006 F., Leuzinger, S., Lucht, W., Medlyn, B., Pfeifer, M., Steinkamp, J., Vanderwel, M. C., Verbeeck, H., and
 1007 Villela, D. M.: Forest resilience and tipping points at different spatio-temporal scales: approaches and
 1008 challenges, *Journal of Ecology*, 103, 5–15, <https://doi.org/10.1111/1365-2745.12337>, 2015.
- 1009 Rosas, T., Mencuccini, M., Barba, J., Cochard, H., Saura-Mas, S., and Martínez-Vilalta, J.: Adjustments and
 1010 coordination of hydraulic, leaf and stem traits along a water availability gradient, *New Phytologist*, 223, 632–
 1011 646, <https://doi.org/10.1111/nph.15684>, 2019.
- 1012 Schenk, H. J.: Soil depth, plant rooting strategies and species’ niches, *New Phytologist*, 178, 223–225,
 1013 <https://doi.org/10.1111/j.1469-8137.2008.02427.x>, 2008.
- 1014 Schenk, H. J. and Jackson, R. B.: The Global Biogeography of Roots, *Ecological Monographs*, 72, 311–328,
 1015 [https://doi.org/10.1890/0012-9615\(2002\)072\[0311:TGBOR\]2.0.CO;2](https://doi.org/10.1890/0012-9615(2002)072[0311:TGBOR]2.0.CO;2), 2002.
- 1016 Schumacher, D. L., Keune, J., Dirmeyer, P., and Miralles, D. G.: Drought self-propagation in drylands due to
 1017 land–atmosphere feedbacks, *Nat. Geosci.*, 15, 262–268, <https://doi.org/10.1038/s41561-022-00912-7>, 2022.
- 1018 Singh, C.: Rooting for forest resilience : Implications of climate and land-use change on the tropical rainforests,
 1019 2023.

- 1020 Singh, C., Wang-Erlandsson, L., Fetzer, I., Rockström, J., and van der Ent, R.: Rootzone storage capacity
 1021 reveals drought coping strategies along rainforest-savanna transitions, *Environ. Res. Lett.*, 15, 124021,
 1022 <https://doi.org/10.1088/1748-9326/abc377>, 2020.
- 1023 Singh, C., van der Ent, R., Wang-Erlandsson, L., and Fetzer, I.: Hydroclimatic adaptation critical to the
 1024 resilience of tropical forests, *Global Change Biology*, 28, 2930–2939, <https://doi.org/10.1111/gcb.16115>, 2022.
- 1025 Singh, V., Karan, S. K., Singh, C., and Samadder, S. R.: Assessment of the capability of SWAT model to
 1026 predict surface runoff in open cast coal mining areas, *Environ Sci Pollut Res*, 30, 40073–40083,
 1027 <https://doi.org/10.1007/s11356-022-25032-y>, 2023.
- 1028 Slik, J. W. F., Franklin, J., Arroyo-Rodríguez, V., Field, R., Aguilar, S., Aguirre, N., Ahumada, J., Aiba, S.-I.,
 1029 Alves, L. F., K, A., Avella, A., Mora, F., Aymard C., G. A., Báez, S., Balvanera, P., Bastian, M. L., Bastin, J.-
 1030 F., Bellingham, P. J., van den Berg, E., da Conceição Bispo, P., Boeckx, P., Boehning-Gaese, K., Bongers, F.,
 1031 Boyle, B., Brambach, F., Brearley, F. Q., Brown, S., Chai, S.-L., Chazdon, R. L., Chen, S., Chhang, P.,
 1032 Chuyong, G., Ewango, C., Coronado, I. M., Cristóbal-Azkarate, J., Culmsee, H., Damas, K., Dattaraja, H. S.,
 1033 Davidar, P., DeWalt, S. J., Din, H., Drake, D. R., Duque, A., Durigan, G., Eichhorn, K., Eler, E. S., Enoki, T.,
 1034 Ensslin, A., Fandohan, A. B., Farwig, N., Feeley, K. J., Fischer, M., Forshed, O., Garcia, Q. S., Garkoti, S. C.,
 1035 Gillespie, T. W., Gillet, J.-F., Gonmadje, C., Granzow-de la Cerda, I., Griffith, D. M., Grogan, J., Hakeem, K.
 1036 R., Harris, D. J., Harrison, R. D., Hector, A., Hemp, A., Homeier, J., Hussain, M. S., Ibarra-Manríquez, G.,
 1037 Hanum, I. F., Imai, N., Jansen, P. A., Joly, C. A., Joseph, S., Kartawinata, K., Kearsley, E., Kelly, D. L.,
 1038 Kessler, M., Killeen, T. J., Kooyman, R. M., Laumonier, Y., Laurance, S. G., Laurance, W. F., Lawes, M. J.,
 1039 Letcher, S. G., Lindsell, J., Lovett, J., Lozada, J., Lu, X., Lykke, A. M., Mahmud, K. B., Mahayani, N. P. D.,
 1040 Mansor, A., Marshall, A. R., Martin, E. H., Calderado Leal Matos, D., Meave, J. A., Melo, F. P. L., Mendoza,
 1041 Z. H. A., et al.: Phylogenetic classification of the world’s tropical forests, *Proceedings of the National Academy
 1042 of Sciences*, 115, 1837–1842, <https://doi.org/10.1073/pnas.1714977115>, 2018.
- 1043 Smith, C. W., Johnston, M. A., and Lorentz, S. A.: The effect of soil compaction on the water retention
 1044 characteristics of soils in forest plantations, *South African Journal of Plant and Soil*, 18, 87–97,
 1045 <https://doi.org/10.1080/02571862.2001.10634410>, 2001.
- 1046 Sperry, J. S. and Love, D. M.: What plant hydraulics can tell us about responses to climate-change droughts,
 1047 *New Phytologist*, 207, 14–27, <https://doi.org/10.1111/nph.13354>, 2015.
- 1048 Staal, A., Tuinenburg, O. A., Bosmans, J. H. C., Holmgren, M., van Nes, E. H., Scheffer, M., Zemp, D. C., and
 1049 Dekker, S. C.: Forest-rainfall cascades buffer against drought across the Amazon, *Nature Climate Change*, 8,
 1050 539–543, <https://doi.org/10.1038/s41558-018-0177-y>, 2018.
- 1051 Staal, A., Fetzer, I., Wang-Erlandsson, L., Bosmans, J. H. C., Dekker, S. C., van Nes, E. H., Rockström, J., and
 1052 Tuinenburg, O. A.: Hysteresis of tropical forests in the 21st century, *Nat Commun*, 11, 4978,
 1053 <https://doi.org/10.1038/s41467-020-18728-7>, 2020.
- 1054 Stevens, B. and Bony, S.: What Are Climate Models Missing?, *Science*, 340, 1053–1054,
 1055 <https://doi.org/10.1126/science.1237554>, 2013.
- 1056 Still, C. J., Berry, J. A., Collatz, G. J., and DeFries, R. S.: Global distribution of C3 and C4 vegetation: Carbon
 1057 cycle implications, *Global Biogeochemical Cycles*, 17, 6-1-6–14, <https://doi.org/10.1029/2001GB001807>,
 1058 2003.
- 1059 Stocker, B. D., Tumber-Dávila, S. J., Konings, A. G., Anderson, M. C., Hain, C., and Jackson, R. B.: Global
 1060 patterns of water storage in the rooting zones of vegetation, *Nat. Geosci.*, 1–7, <https://doi.org/10.1038/s41561-023-01125-2>, 2023.
- 1062 Sveen, T. R., Hannula, S. E., and Bahram, M.: Microbial regulation of feedbacks to ecosystem change, *Trends
 1063 in Microbiology*, 32, 68–78, <https://doi.org/10.1016/j.tim.2023.06.006>, 2024.

- 1064 Trumbore, S., Brando, P., and Hartmann, H.: Forest health and global change, *Science*, 349, 814–818,
1065 <https://doi.org/10.1126/science.aac6759>, 2015.
- 1066 Valdes, P.: Built for stability, *Nature Geosci*, 4, 414–416, <https://doi.org/10.1038/ngeo1200>, 2011.
- 1067 Wang, E., Smith, C. J., Wang, E., and Smith, C. J.: Modelling the growth and water uptake function of plant
1068 root systems: a review, *Aust. J. Agric. Res.*, 55, 501–523, <https://doi.org/10.1071/AR03201>, 2004.
- 1069 Wang-Erlandsson, L., Bastiaanssen, W. G. M., Gao, H., Jägermeyr, J., Senay, G. B., van Dijk, A. I. J. M.,
1070 Guerschman, J. P., Keys, P. W., Gordon, L. J., and Savenije, H. H. G.: Global root zone storage capacity from
1071 satellite-based evaporation, *Hydrology and Earth System Sciences*, 20, 1459–1481,
1072 <https://doi.org/10.5194/hess-20-1459-2016>, 2016.
- 1073 Wang-Erlandsson, L., Tobian, A., van der Ent, R. J., Fetzer, I., te Wierik, S., Porkka, M., Staal, A., Jaramillo,
1074 F., Dahlmann, H., Singh, C., Greve, P., Gerten, D., Keys, P. W., Gleeson, T., Cornell, S. E., Steffen, W., Bai,
1075 X., and Rockström, J.: A planetary boundary for green water, *Nat Rev Earth Environ*, 3, 380–392,
1076 <https://doi.org/10.1038/s43017-022-00287-8>, 2022.
- 1077 Wolfe, B. T., Sperry, J. S., and Kursar, T. A.: Does leaf shedding protect stems from cavitation during seasonal
1078 droughts? A test of the hydraulic fuse hypothesis, *New Phytologist*, 212, 1007–1018,
1079 <https://doi.org/10.1111/nph.14087>, 2016.
- 1080 Wunderling, N., Staal, A., Sakschewski, B., Hirota, M., Tuinenburg, O. A., Donges, J. F., Barbosa, H. M. J.,
1081 and Winkelmann, R.: Recurrent droughts increase risk of cascading tipping events by outpacing adaptive
1082 capacities in the Amazon rainforest, *Proceedings of the National Academy of Sciences*, 119, e2120777119,
1083 <https://doi.org/10.1073/pnas.2120777119>, 2022.
- 1084 Xie, S.-P., Deser, C., Vecchi, G. A., Ma, J., Teng, H., and Wittenberg, A. T.: Global Warming Pattern
1085 Formation: Sea Surface Temperature and Rainfall, *Journal of Climate*, 23, 966–986,
1086 <https://doi.org/10.1175/2009JCLI3329.1>, 2010.
- 1087 Xu, C., Hantson, S., Holmgren, M., van Nes, E. H., Staal, A., and Scheffer, M.: Remotely sensed canopy height
1088 reveals three pantropical ecosystem states, *Ecology*, 97, 2518–2521, <https://doi.org/10.1002/ecy.1470>, 2016.
- 1089 Xue, B.-L., Guo, Q., Otto, A., Xiao, J., Tao, S., and Li, L.: Global patterns, trends, and drivers of water use
1090 efficiency from 2000 to 2013, *Ecosphere*, 6, art174, <https://doi.org/10.1890/ES14-00416.1>, 2015.
- 1091 Yang, Y., Saatchi, S. S., Xu, L., Yu, Y., Choi, S., Phillips, N., Kennedy, R., Keller, M., Knyazikhin, Y., and
1092 Myneni, R. B.: Post-drought decline of the Amazon carbon sink, *Nat Commun*, 9, 3172,
1093 <https://doi.org/10.1038/s41467-018-05668-6>, 2018.
- 1094 Yu, Z., Chen, X., Zhou, G., Agathokleous, E., Li, L., Liu, Z., Wu, J., Zhou, P., Xue, M., Chen, Y., Yan, W.,
1095 Liu, L., Shi, T., and Zhao, X.: Natural forest growth and human induced ecosystem disturbance influence water
1096 yield in forests, *Commun Earth Environ*, 3, 148, <https://doi.org/10.1038/s43247-022-00483-w>, 2022.
- 1097 Yuan, K., Zhu, Q., Riley, W. J., Li, F., and Wu, H.: Understanding and reducing the uncertainties of land
1098 surface energy flux partitioning within CMIP6 land models, *Agricultural and Forest Meteorology*, 319, 108920,
1099 <https://doi.org/10.1016/j.agrformet.2022.108920>, 2022.
- 1100 Zemp, D. C., Schleussner, C.-F., Barbosa, H. M. J., van der Ent, R. J., Donges, J. F., Heinke, J., Sampaio, G.,
1101 and Rammig, A.: On the importance of cascading moisture recycling in South America, *Atmospheric
1102 Chemistry and Physics*, 14, 13337–13359, <https://doi.org/10.5194/acp-14-13337-2014>, 2014.

- 1103 Zemp, D. C., Schleussner, C.-F., Barbosa, H. M. J., Hirota, M., Montade, V., Sampaio, G., Staal, A., Wang-
1104 Erlandsson, L., and Rammig, A.: Self-amplified Amazon forest loss due to vegetation-atmosphere feedbacks,
1105 Nature Communications, 8, 14681, <https://doi.org/10.1038/ncomms14681>, 2017.
- 1106 Zhang, Y., Peña-Arancibia, J. L., McVicar, T. R., Chiew, F. H. S., Vaze, J., Liu, C., Lu, X., Zheng, H., Wang,
1107 Y., Liu, Y. Y., Miralles, D. G., and Pan, M.: Multi-decadal trends in global terrestrial evapotranspiration and its
1108 components, Scientific Reports, 6, 19124, <https://doi.org/10.1038/srep19124>, 2016.
- 1109 Zilli, M. T., Carvalho, L. M. V., and Lintner, B. R.: The poleward shift of South Atlantic Convergence Zone in
1110 recent decades, Clim Dyn, 52, 2545–2563, <https://doi.org/10.1007/s00382-018-4277-1>, 2019.
- 1111
- 1112



1114

1115

1116

1117

1118

1119

1120

1121

1122

1123

1124

1125

1126

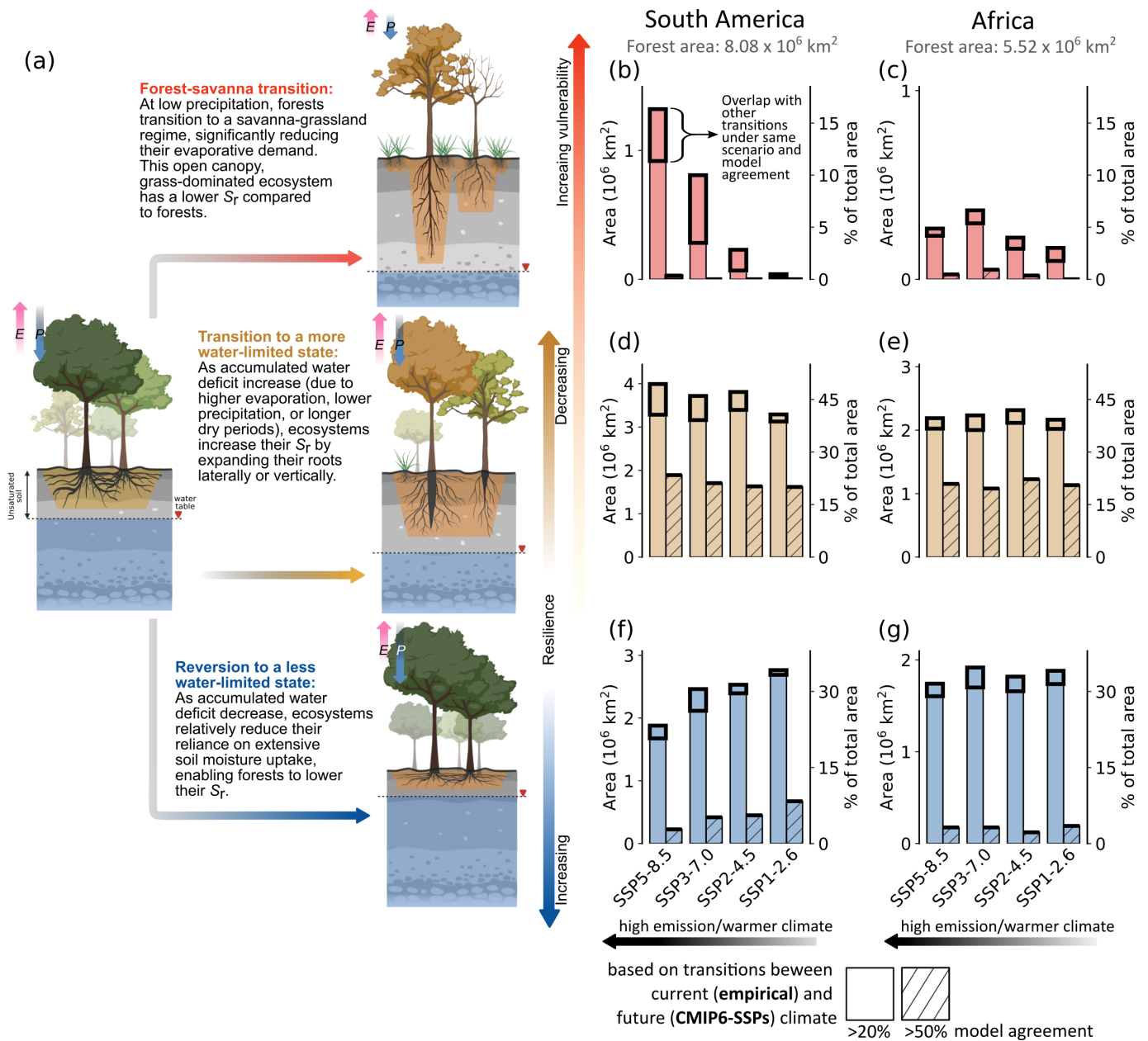
1127

1128

1129

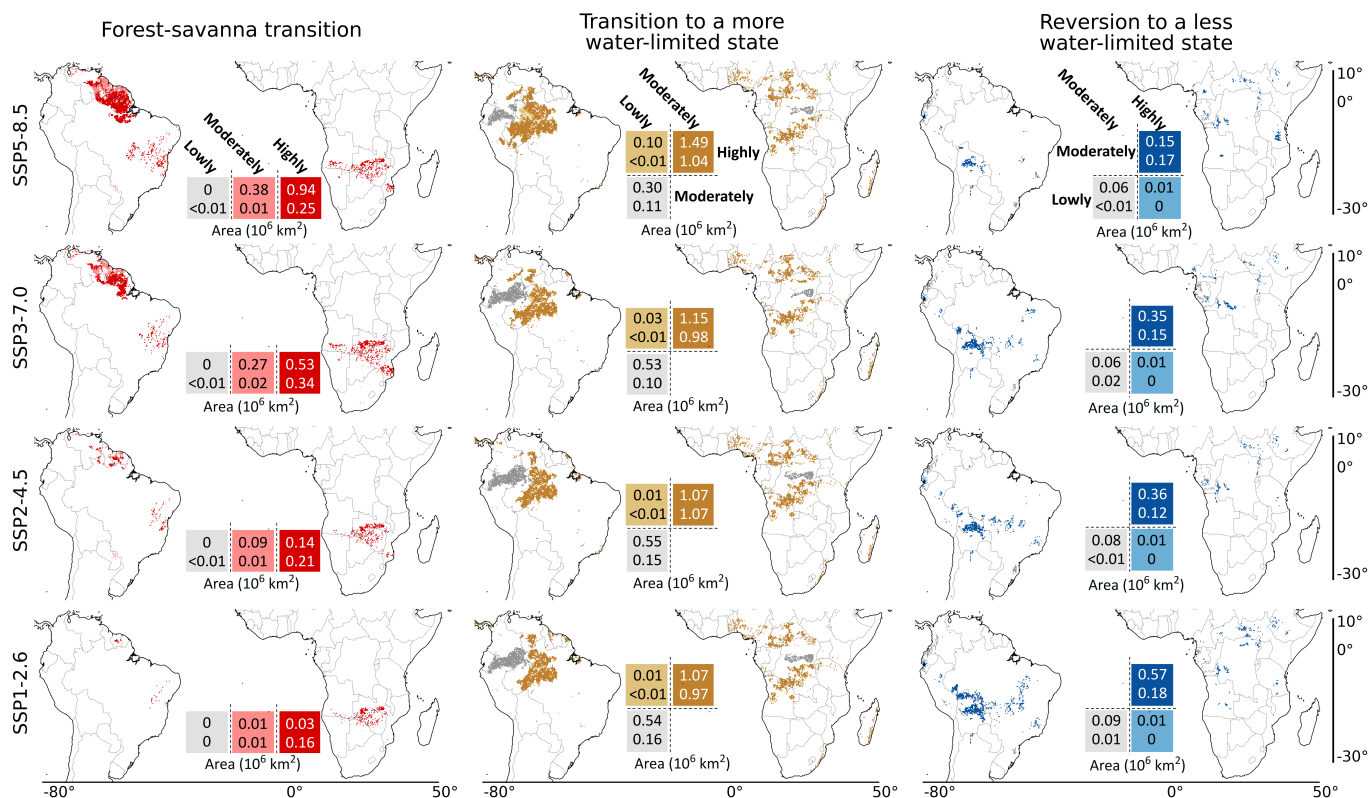
1130

Figure 1: Methodological framework for analysing the potential transitions in tropical terrestrial ecosystems using empirical and CMIP6-Earth System Models (ESMs) hydroclimate estimates. (a) We use root zone storage capacity (S_r)-based classification thresholds (obtained from Singh et al., 2020) – calculated using empirical precipitation (P) and evaporation (E) estimates (Fig. S1; see Methodology section and Appendix A1) – to classify terrestrial ecosystems under the current climate. Savanna ecosystems under the current climate are excluded from this analysis. We bias-correct these S_r thresholds for all ESMs using the histogram equivalence method (Piani et al., 2010) (Table S1). (b) We then use these bias-corrected S_r thresholds to classify ecosystems under future climate conditions (Fig. S2 and S3). Furthermore, we use mean annual precipitation (\bar{P}) and P -seasonality index range (S_r -based forest classes from a) - as a proxy for ecosystem state - to revise our classification under future climate (Appendix A3 and Fig. S4). (c) We then analyse the potential transitions by comparing ecosystems classified under the current climate (analysed in a) with those classified under future climate (analysed in b) individually for all ESMs (Fig. S5 and S6). The transition analysis assumes that the hydroclimate and the ecosystem are in equilibrium, and does not account for the time required for transitions to occur. A detailed description is provided in the Methodology section. An exemplification of this methodological framework is shown in Fig. S7.

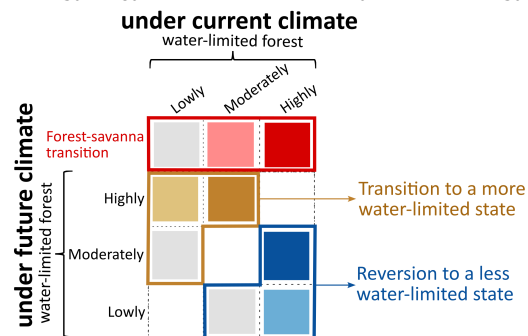


1131
 1132 **Figure 2: Comparing the potential transitions under different SSP scenarios.** (a) The state of the ecosystem, both above- and below-ground, (post-transition) under future climate, quantifying (b,c) forest-savanna transition,
 1133 (d,e) forests' that transition to a more water-limited state and (f,g) revert to a less water-limited state for South America and Africa (present forest area mentioned on the top of (b,c)), respectively. For the analysis above,
 1134 transitions are calculated for grid cells with model agreement >20% (plain bar plot) and >50% (hatched bar plot). These quantifications show changes in the forest area based on ecosystem transitions under empirical-current
 1135 (2001-2012) and future (2086-2100) climate conditions. For all these transitions, we assume that the hydroclimate and the ecosystem are in equilibrium. Analyses comparing ecosystem transitions based on CMIP6-historical
 1136 (2000-2014) and future (2086-2100) climate conditions are shown in Fig. S10 and S11. For each transition, the total area of spatial overlap with other transitions under the same SSP scenario and model agreement
 1137 is highlighted with thick black bars. The P and E arrows in (a) describe the relative magnitude of precipitation and evaporation fluxes. The illustration in (a) is adapted from Singh et al. (2020) and created with [BioRender.com](https://www.biorender.com).
 1138
 1139
 1140
 1141
 1142
 1143

1144



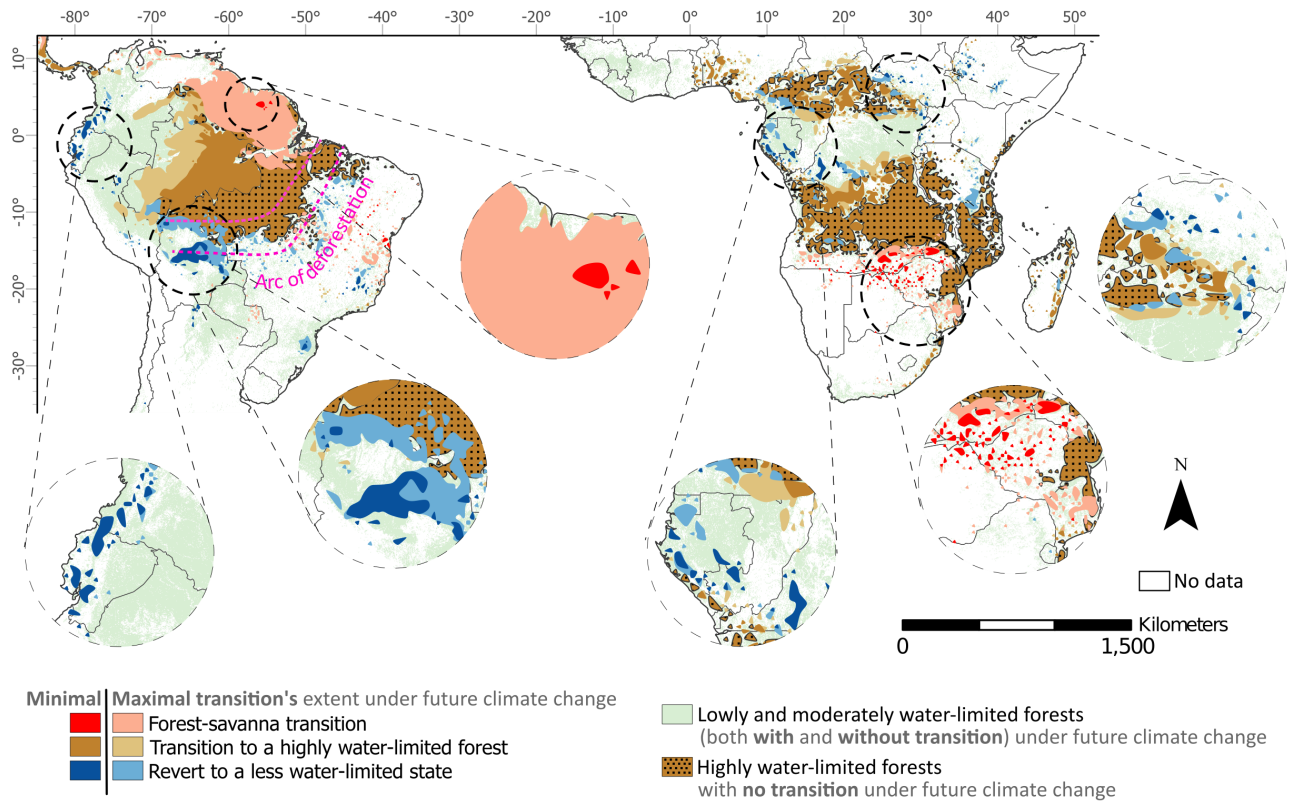
Total forest area for South America: $8.08 \times 10^6 \text{ km}^2$
and Africa: $5.52 \times 10^6 \text{ km}^2$



1145

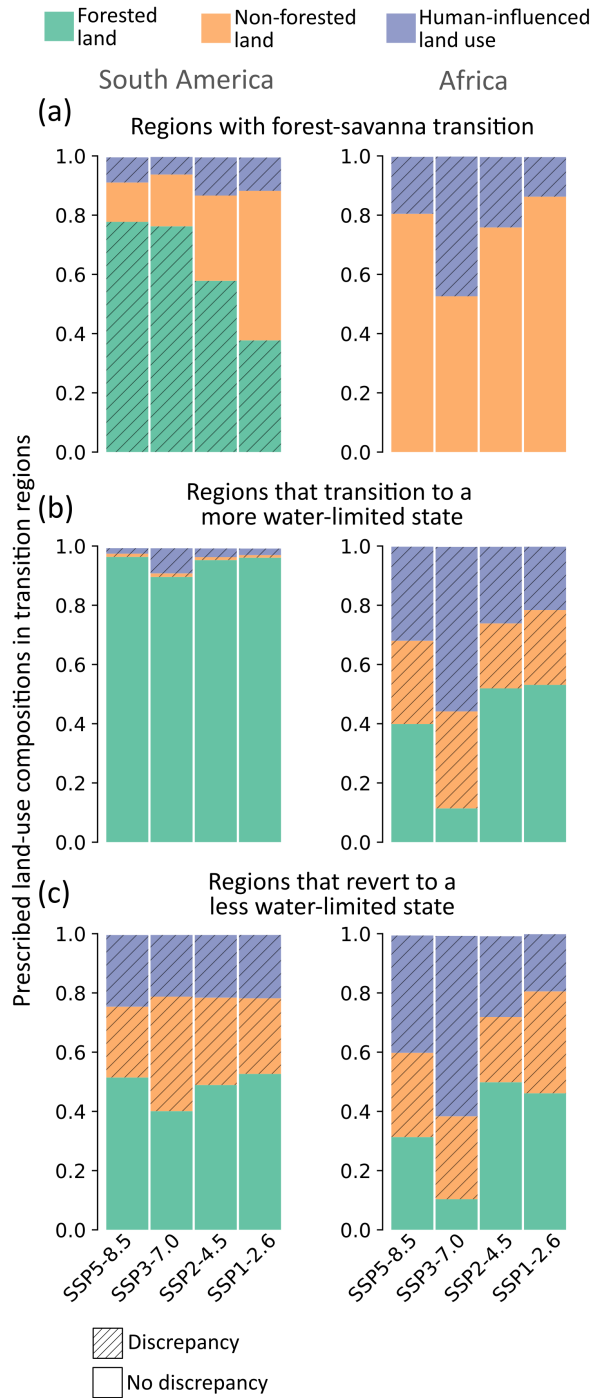
1146 **Figure 3: Spatial extent of potential transitions with respect to their current state under different SSP**
 1147 **scenarios.** We analysed transitions, explicitly focusing on forest-savanna transition, transition to a more
 1148 water-limited state, and reversion to a less water-limited state, by comparing different ecosystem classes under current
 1149 (empirical; 2001-2012) and future (SSPs; 2086-2100) climate conditions (as defined in Fig. 2). All transitions
 1150 shown above are analysed for moderate-high (>50%) model agreement, except forest-savanna transition, for
 1151 which moderate (>20%) model agreement is considered. Values overlaying the legends correspond to the total
 1152 area of transition for South America (top values) and Africa (bottom values).

1153



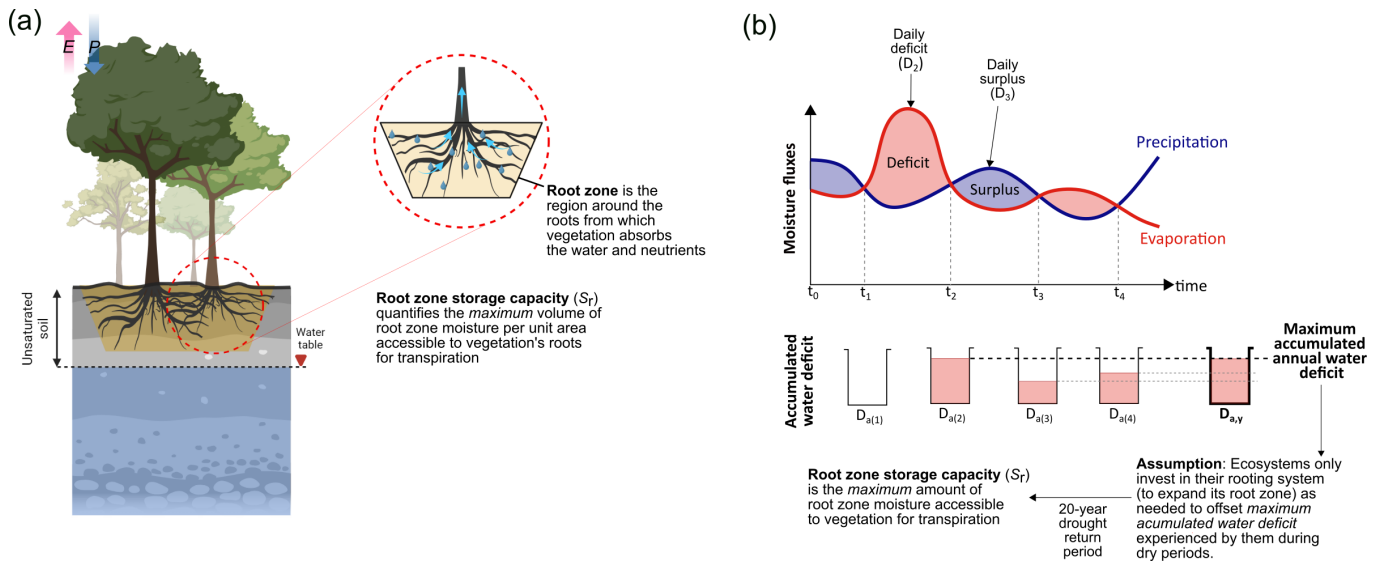
1154
 1155 **Figure 4: Minimal and maximal extent of potential ecosystem transitions under future climate change in**
 1156 **the entire study region over South America and Africa.** The three transition types are: forest-savanna
 1157 transition, from any class to highly water-limited forests, and to a less water-limited state (see definitions in Fig.
 1158 2 and 3). For better visualisation of these transitions, in this figure, we first converted all grid cells to shape,
 1159 merged them, and then smoothed them using the 'polynomial approximation with exponential kernel' function
 1160 (with a tolerance value of 1) in ArcGIS pro. The unsmoothed version of the transitions is shown in Fig. 3. The
 1161 minimal and maximum represent the minimum and maximum possible extent of transitions (as quantified in Fig.
 1162 3) based on changes between current (empirical; 2001-2012) and future (SSPs; 2086-2100) climate conditions
 1163 regardless of the SSP scenarios.

1164



1165
 1166 **Figure 5: Prescribed land-use composition for each transition region under different SSP scenarios**
 1167 **(median 2086-2100), calculated as the ratio between the prescribed land use area and the projected**
 1168 **transition area.** Regions where IAM prescribed land use are same as the projected transitions (from Fig. 3)
 1169 are shown in plain colours (i.e., no discrepancy). Whereas regions where IAM-prescribed land use differs from
 1170 projected transitions are hatched (i.e., discrepancy).

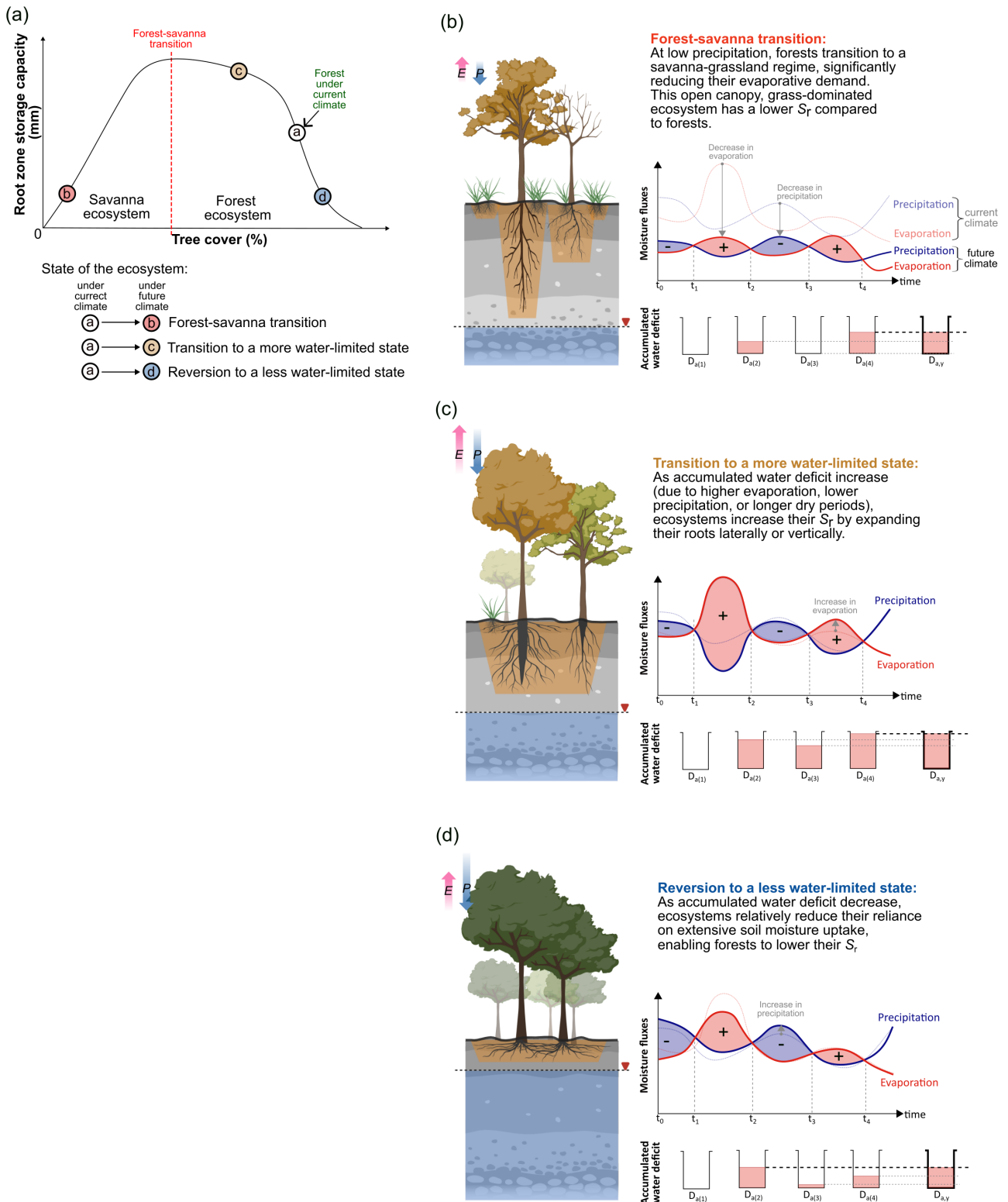
1171



1172

1173 **Figure A1:** The figure illustrates the root zone storage capacity (S_r) of the ecosystem. (a) We show the difference
 1174 between the ecosystem's root zone and how that constitutes its S_r . (b) Conceptual illustration of how the
 1175 ecosystem's precipitation and evaporation fluxes constitute the maximum accumulated annual water deficit ($D_{a,y}$)
 1176 and S_r . The figure is adopted from Singh (2023) and Wang-Erlandsson et al. (2016).

1177



1178

1179 **Figure A2:** (a) The figure compares the root zone storage capacity (S_r) with the ecosystem state (i.e., tree cover).
 1180 This figure expands on the conceptual illustration from Fig. A1, showing how the ecosystem's precipitation and
 1181 evaporation fluxes contribute to S_r under different forest transition scenarios: (b) forest-savanna transition, (c)
 1182 transition to a more water-limited state, and (d) reversion to a less water-limited state.

1183